

Hierarchically structured bioinspired nanocomposites

Received: 12 December 2020

Accepted: 17 September 2022

Published online: 28 November 2022

 Check for updates

Dhriti Nepal¹✉, Saewon Kang², Katarina M. Adstedt², Krishan Kanhaiya³, Michael R. Bockstaller⁴, L. Catherine Brinson⁵, Markus J. Buehler⁶, Peter V. Coveney⁷, Kaushik Dayal⁸, Jaafar A. El-Awady⁹, Luke C. Henderson¹⁰, David L. Kaplan¹¹, Sinan Keten¹², Nicholas A. Kotov¹³, George C. Schatz¹⁴, Silvia Vignolini¹⁵, Fritz Vollrath¹⁶, Yusu Wang¹⁷, Boris I. Yakobson^{18,19}, Vladimir V. Tsukruk²✉ & Hendrik Heinz³✉

Next-generation structural materials are expected to be lightweight, high-strength and tough composites with embedded functionalities to sense, adapt, self-repair, morph and restore. This Review highlights recent developments and concepts in bioinspired nanocomposites, emphasizing tailoring of the architecture, interphases and confinement to achieve dynamic and synergetic responses. We highlight cornerstone examples from natural materials with unique mechanical property combinations based on relatively simple building blocks produced in aqueous environments under ambient conditions. A particular focus is on structural hierarchies across multiple length scales to achieve multifunctionality and robustness. We further discuss recent advances, trends and emerging opportunities for combining biological and synthetic components, state-of-the-art characterization and modelling approaches to assess the physical principles underlying nature-inspired design and mechanical responses at multiple length scales. These multidisciplinary approaches promote the synergetic enhancement of individual materials properties and an improved predictive and prescriptive design of the next era of structural materials at multilength scales for a wide range of applications.

In an evolutionary process over millions of years, nature has mastered the fabrication of hierarchical multifunctional materials that in many ways surpass their synthetic counterparts^{1,2}. The astonishing results have been achieved by taking advantage of diverse fundamental molecular interactions among a small set of building blocks under ambient conditions (Box 1). In particular, the evolutionary development of multi-layer hierarchical structures with unique and sometimes contradictory properties, such as combined high strength and toughness, provides great inspiration for modern materials engineering. Mimicking nature's hierarchical microstructures in synthetic composites can lead to more damage-tolerant architectures, and some bioinspired materials have already been implemented in various applications³. To advance, the field requires the development of sustainable, hierarchical and dynamic

composites that are multifunctional and environmentally friendly. However, the engineering of bioinspired structures faces many challenges, including the realization of molecular-scale precision within each level of the hierarchy, structural coupling between hard and soft building blocks, the retention of mechanical integrity while achieving a good balance of other functional properties, and the capacity for fast and large-scale production.

One great challenge for the development of bioinspired composites is to gain control over the composition, gradients, interfaces, microstructures, morphology and responses under dynamic conditions. In certain instances, synthetic composites are superior to bioinspired composites, for example, in the automotive and aerospace field where temperature resistance is critical. Yet, bioinspired composites can be

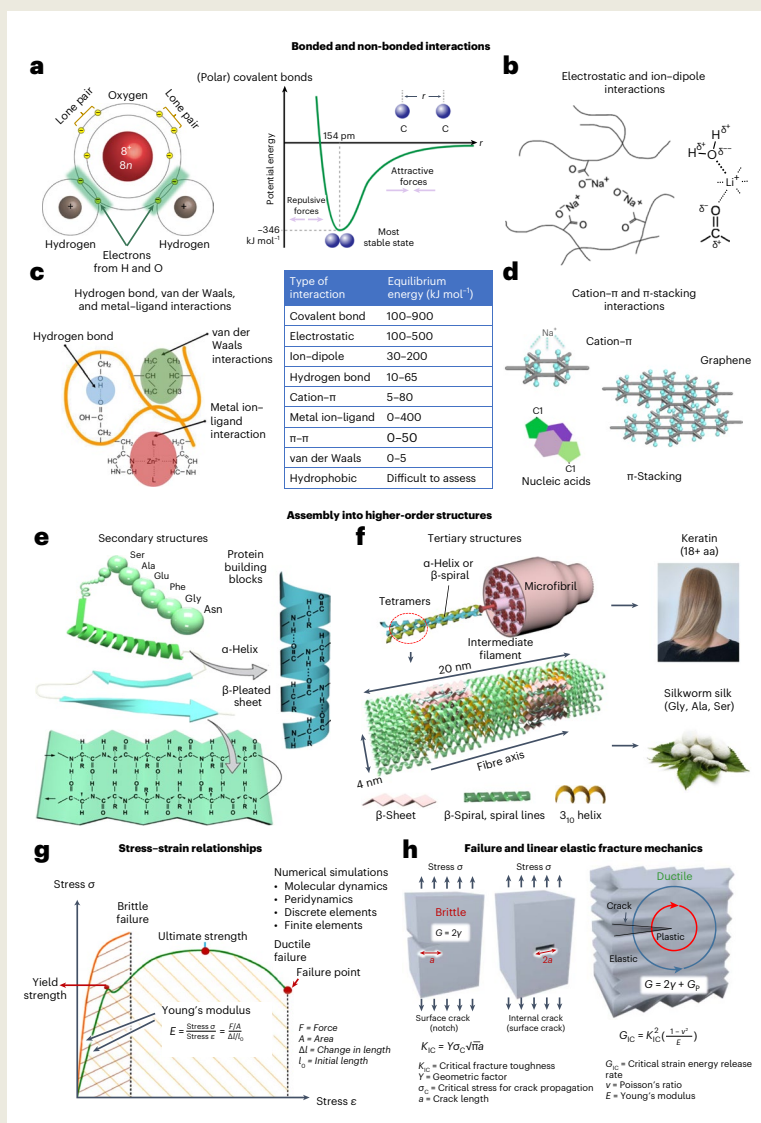
A full list of affiliations appears at the end of the paper. ✉ e-mail: dhriti.nepal.1@afri.af.mil; vladimir@mse.gatech.edu; hendrik.heinz@colorado.edu

BOX 1

Hierarchical structures and mechanical behaviour

The primary structures of inorganic and organic compounds are determined by chemical and physical interactions of various strengths (**a–d**)¹²⁶. The molecular structure usually involves covalent bonds of varying polarity, as shown for water (**a**, left). The potential energy as a function of distance between two atoms resembles a Morse potential, shown for a C–C single bond (**a**, right). Molecular structures are also influenced by non-covalent interactions such as electrostatic (**b**), hydrogen-bonding, van der Waals, metal ion–ligand (**c**), cation– π and π -stacking interactions (**d**). Inter- and intramolecular interactions at the weaker end of the energy spectrum are thermally and mechanically reconfigurable and play a major role in generating cohesion via large numbers of interactions across material volumes. The full set of bonding and non-bonding interactions, the specific chemistry and solution conditions such as pH direct the folding and assembly of larger molecules, inorganic components, and building blocks into higher-order structures (**e** and **f**). For example, the sequence of covalently bonded amino acids and the pattern of hydrogen bonds in proteins determine

the formation of random coil, α -helix, β -sheet and other organized building blocks (**e**). These nanometre-scale units can organize into hierarchical structures, for example, α -helical supercoils in keratin and a combination of β -spirals and β -sheet nanocrystals in silk fibrils, which provides mechanical reinforcement (**f**)⁸. The key mechanical properties are derived from stress–strain curves, which are obtained by gradually applying a load (stress) to a test sample and measuring the deformation (strain; **g**). The propagation of cracks and failure in materials can be analysed by fracture mechanics (**h**)¹⁰⁸. Brittle materials fail by crack propagation, whereas ductile materials undergo additional plastic deformation, including craze formation in polymers near the crack tip. Crack growth in brittle materials occurs when the increase in the surface energy γ of cracks is compensated by a decrease in strain energy via stress release (Griffith theory, total energy for crack growth $G=2\gamma$). In ductile materials, the total free energy for crack growth is dominated by plastic deformation G_p and follows the more general Irwin theory ($G=2\gamma+G_p$). Credit (silkworm and silk cocoon in **f**): Alamy.



produced under ecofriendly conditions by combining traditional design strategies and advanced synthetic materials, resulting in exceptional properties. Studies on some of the most robust natural materials have provided insights into the basic principles of design, especially the critical role of molecular interactions and hierarchical architectures (panels a–f in Box 1)^{2,4}. Structural hierarchy enables multiple deformation, self-healing, plasticity and toughening mechanisms within the composites across length scales⁵. For example, at the nanometre scale, the architectures of compositional gradients and fuzzy interphases (three-dimensional (3D) interfacial regions), as discovered in layer-by-layer assembled structures, facilitate intrinsic toughening by chain slippage, stress delocalization and non-destructive locking across organic interfaces. Simultaneously, at the larger micrometre scale, hierarchical structures play a pivotal role in extrinsic toughening, for example, crack-bridging and pull-out to dissipate energy via weak or soft interfaces (see the fundamental relationships highlighted in panels g and h in Box 1)^{1,4}. To harness such functions, many organisms have developed an unparalleled ability to shape mineral-rich materials into anisotropic structures to serve as load-bearing elements that extend over several orders of magnitude in size⁶. The resulting combination of stiffness, strength and toughness has fuelled research into synthetic bioinspired analogues because existing synthetic composite materials often show increased strength at the expense of toughness or vice versa.

A second great challenge in the modern materials world, drawing inspiration from nature, is to master scale-up synthesis and processing in industrial settings, including added functionality in structural components⁷. Multifunctional hierarchical materials found in plants and living organisms include celluloses, keratins and silk (Fig. 1 and panels e and f in Box 1). These complex systems are produced in nature at a massive scale and engineered using relatively simple building blocks and constituents under highly sustainable conditions, including aqueous environments and ambient temperature.

We specifically highlight keratin, a critical component of many natural structures, as an inspirational resource (Fig. 1)⁸. Keratin is a structural protein in hair, horn and hoof (panel f in Box 1) that serves as a robust yet soft material in the exoskeleton of a wide range of vertebrates (Fig. 1). The exoskeleton of animals exhibits multiple functions: self-defence, communication, sensing and temperature regulation, albeit each process uses different mechanisms facilitated by complex hierarchical structures and composition gradients. We can categorize examples of these keratin-based multifunctional hierarchical structures from six distinct animal species into two primary functions: mechanics and photonics (Fig. 1). One major function of horn and hoof is impact resistance and energy absorption⁹. More subtly, keratin functions as a defensive shield in pangolin scales through a complex curved architecture (Fig. 1a)⁸, a piercing weapon in porcupine quills (Fig. 1b)⁸, and sturdy protection through ordered stacks in turtle shells (Fig. 1c)¹⁰ and rhinoceros horn (Fig. 1d)¹¹. These hierarchical structures have a variety of shapes, such as the waved stripes of cellular morphology in multilayered laminates (Fig. 1a), amorphous foams (Fig. 1b), microplatelet-containing lamellae of turtle shells (Fig. 1c) and curved lamellar pillars in rhinoceros horns (Fig. 1d). All these hierarchical structures achieve the function of dissipating energy for self-defence. In one specific structure, the pangolin scale's multilayered laminates, the lamellar structures exhibit unusual crack deflection with non-uniform crack profiles (Fig. 1a). Interlamellar shearing of the keratin interfaces leads to tablet sliding and inelastic regions surrounding cracks, resulting in enhanced fracture toughening¹². The microtubule structures serve as a stiff reinforcement that supports the entire wall and prevents catastrophic failure under impact loading via the inherently viscoelastic properties of keratin⁹. These hierarchical layered architectures are necessary for penetration resistance and dissipating energy within the sublayers, helping to delocalize stresses and damages while being environmentally resilient under extreme fluctuations in humidity and temperature.

In contrast to direct structural applications related to self-defence, keratin can be combined with periodic inclusions of melanin rods to form photonic crystals with the bright, vivid colouration found in many bird feathers, including peacock feathers (Fig. 1e). Keratin can also protect the structure of guanine nanocrystals for colour adaptivity in the chameleon dermis (Fig. 1f)¹³. Both of these photonic structures use fibrillar architectures, as seen by the organized fibrils and pores in peacock feather frames (Fig. 1e), and the multiple sheets and fibrils in chameleon skin (Fig. 1f). These complex keratin-based hierarchical structures illustrate examples of multifunctionality while being mechanically resilient^{9,12}, fulfilling essential roles for defence, stress signalling, courtship display through structural colour and thermal protection¹³.

Elucidating the underlying mechanisms and correlated functions of such complex structures still poses a tremendous challenge for the scientific community. Understanding the design principles provides opportunities to incorporate various functions such as photonics and morphing into synthetic systems while enhancing mechanical integrity. The goal of 'emulating nature's design principles' can also be accelerated through interactive, real-time feedback in synthesis and characterization by using opportunities in artificial intelligence (AI), including machine learning (ML), data science methods and additive manufacturing.

On the basis of the structure–function prototypes found in nature and recent studies, this Review examines recent breakthroughs, trends and advances in the design, synthesis and understanding of nature-inspired hierarchical materials. We emphasize how weak and strong chemical interactions can be configured to create synthetic hierarchical architectures with tight control over morphology, structure, function, appearance and mechanics at different length, time and force scales. We identify critical challenges for the design of future structural materials with added functionalities and discuss how an interdisciplinary era of materiomics that harnesses big data could accelerate the development of the next generation of advanced materials by linking material structure to properties and functions.

Hierarchical interactions across scales

The unique combination of mechanical and functional properties in natural materials is associated with hierarchical organization at various length scales, which can also change with time, from molecular ordering to macroscale assembly (Fig. 2, Hierarchical structures). Such synergetic self-organization is mediated by ubiquitous, highly structured, hard/soft interfaces¹⁴. A common feature of these interfaces is 'deliberate imperfection', that is, a designed degree of complexity not found in engineered materials.

The spatial dimensions of hierarchical structures vary greatly from zero-dimensional (0D) to *N*-dimensional (*ND*), depending on the end-goal functionality and volume constraints. *ND* structures may also incorporate further dimensions such as time or other responsive changes in the material. The dimensions of these *ND* structures further influence the size and subsequent interactions of the molecules and interfaces, as well as the eventual, multilevel, macroscale material structure, such as twisted, laminated or fibrous composites (Hierarchical structures in Fig. 2). Hierarchical structures can span beyond singular dimensions, as evidenced by the organization of peptides into nanoscale sheets and their subsequent organization into fibrillar structures that bundle to form large-scale fibrillar and laminated solids (Hierarchical structures in Fig. 2a–e). The assembly into laminated and fibrillar structures defines a higher level of organization of interfaces and nanostructures in large-scale bioinspired and synthetic inorganic–organic materials (Hierarchical structures in Fig. 2f–n).

Ultimately, the combination of strong and weak interfaces determines the toughness, strength and stiffness of a material, along with its shear and adhesive properties (Global functions in Fig. 2, two top panels). A prominent example from nature that uses strong

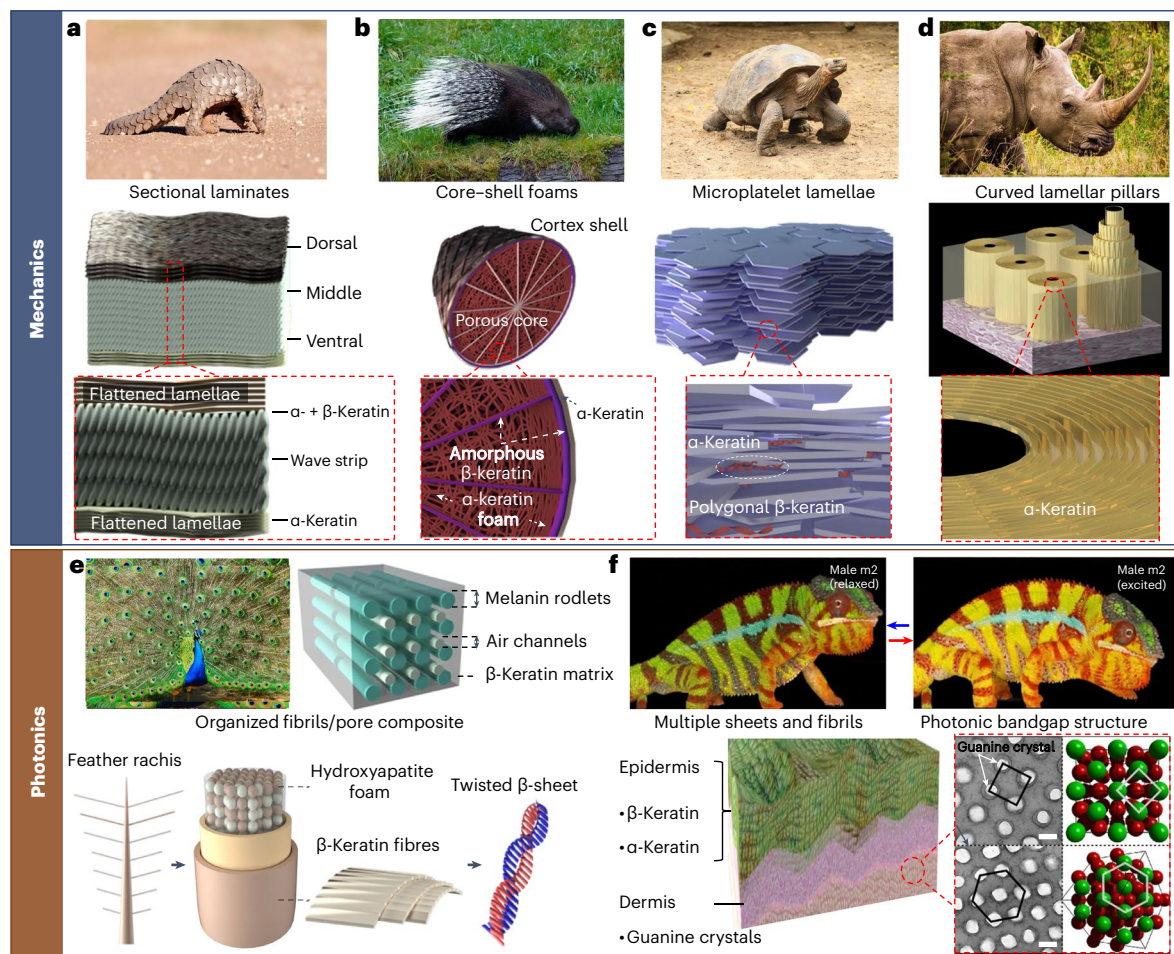


Fig. 1 | Keratin-based hierarchical structures in different animal species.

A common feature of keratin-based hierarchical composites is their precisely folded tertiary keratin structure, which controls mechanics by means of layers, interfaces and gradients, as well as their co-assembly with other functional polymers or minerals to generate periodic order. **a**, Pangolin scales consist of α - and β -keratin and are known for their distinctive protection mechanism. The scales comprise an internal layered structure with densely packed keratinized flattened lamellae that are wavy and parallel to the external surface in the dorsal and ventral regions, and an elongated cellular morphology that is tilted and deformed in the middle region⁸. **b**, Porcupine quills are composed of a keratin configuration that includes a stiff outer sheath and compliant porous core structure⁸. **c**, Turtle shells are biomineralized structures constructed from compacted, ordered and stacked polygonal keratin microlamellae that have a high amount of β -keratin and a small quantity of α -keratin and minerals (calcium phosphate and calcium sulfate)⁹. **d**, Rhinoceros horns are made of α -keratin with a lamellar structure (2–5 μm in thickness) stacked in the radial direction with tubules (40–100 μm in diameter) dispersed between the lamellae, extending along the length of the horn in the growth direction¹⁰.

e, Peacock tail feathers are composed of parallel melanin rod bundles connected in a β -keratin matrix to yield a 2D photonic structure that generates magnificent iridescent colours. The feather rachis contains branches of multicoloured barbs that derive their unique iridescence from parallel oriented bundles of fibrils composed of two twisted β -sheets consisting mostly of hydroxyapatite foam and a small portion of cortex from β -keratin fibres⁸. **f**, The panther chameleon shows a beautiful striped green pattern due to photonic guanine crystals in the relaxed state. The colour changes to a bright yellow in the stressed state. The epidermis consists of highly keratinized layers of α - and β -keratin that give the skin a rough texture, defend against predators and protect the softer and more adaptive photonic crystals underneath the epidermis¹¹. Scale bars, 200 nm. Credit (top images in **a–e**): (Ben McRae / Alamy Stock Photo (**a**); pangolin); Prisma by Dukas Presseagentur GmbH / Alamy Stock Photo (**b**); porcupine); C. Storz / Alamy Stock Photo (**c**); tortoise); aroundtheworld.photography / Alamy Stock Photo (**d**); rhinoceros); aroundtheworld.photography / Alamy Stock Photo (**e**); peacock). Panel **f** adapted with permission from ref. ¹³ under a Creative Commons licence [CC BY 4.0](https://creativecommons.org/licenses/by/4.0/).

and weak interfaces for energy dissipation is nacre, which features a ‘brick-and-mortar’ configuration with relatively stiff aragonite bricks and soft biological material as the mortar. A small fraction (~5%) of protein binder is sufficient to notably increase fracture toughness as it allows the aragonite bricks to slide, dissipating energy while retaining an overall high stiffness¹⁵. Reversible reorganization of interfaces, driven by induced phase and molecular transformations, facilitates a dynamic behaviour that allows nature to modulate shape and stimuli-responsive properties (two bottom panels in Global functions in Fig. 2). Morphing and responsive behaviour are realized by a variety of molecular mechanisms, such as the realignment or

rebonding of functional groups, molecules and nanoparticles. The processes of bonding, reaction, relaxation and diffusion of structural elements range from picosecond to millisecond timescales (Time-scale and interactions in Fig. 2). Furthermore, material-forming processes include aggregation, crystallization, dissolution, phase separation, relaxation, controlled deformation, appearance, morphing and self-healing of hierarchical materials across similar timescales.

Therefore, it is challenging to develop synthetic hierarchical structures with the mechanical resilience (panel **g** in Box 1) and functionalities that nature can offer¹⁶. It remains difficult to

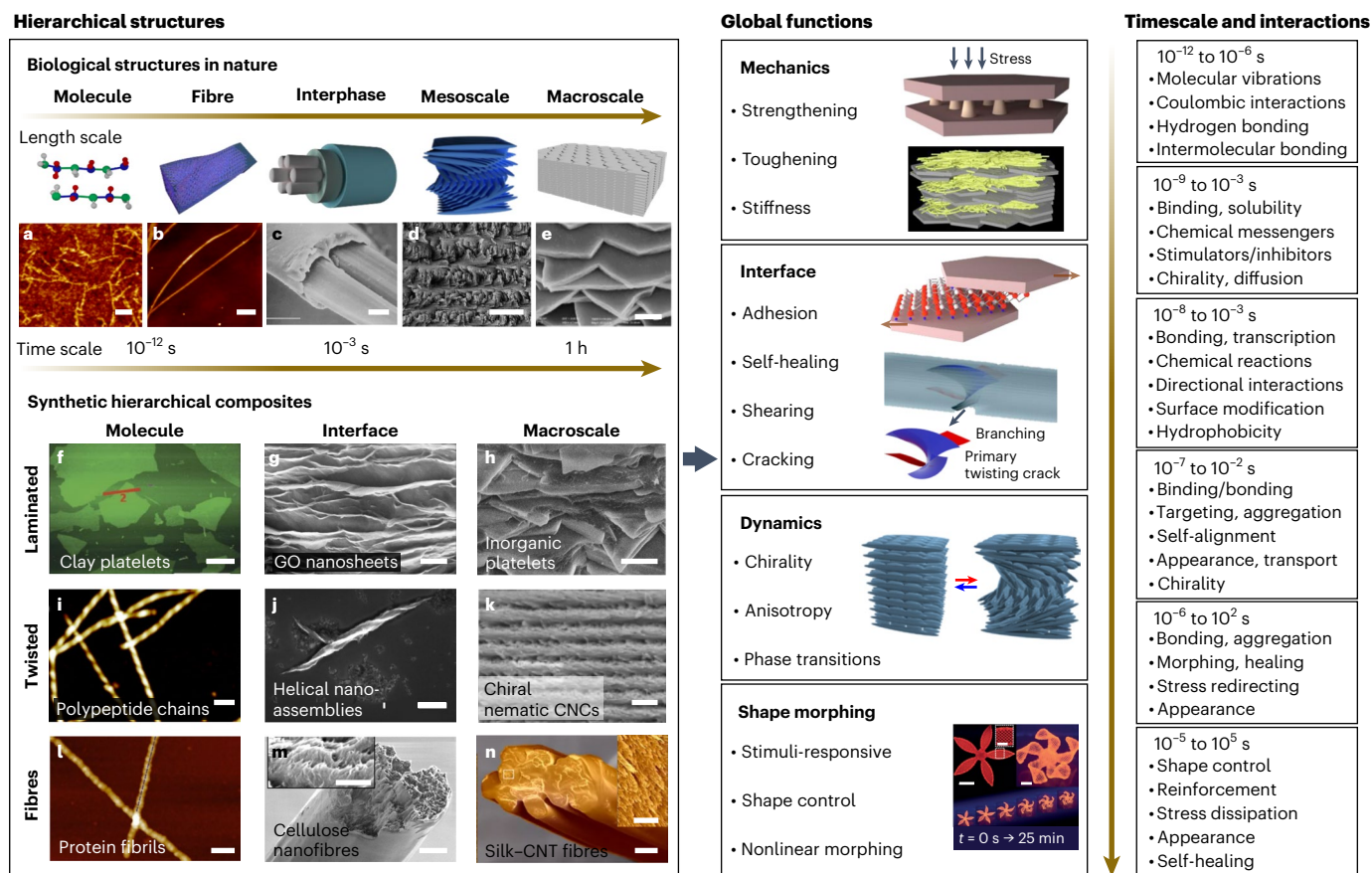


Fig. 2 | Hierarchical bioinspired composite designs in terms of space and time, and major contributions in mechanical functionality. Top left: representative hierarchical biological structures from nature, showing schematics (top) and actual morphologies (bottom). **a**, Atomic force microscopy (AFM) topographical image of the β -sheet secondary structure of silk fibroin¹¹. **b**, AFM topographical image of silk nanofibrils¹². **c**, Scanning electron microscopy (SEM) image of single-filament silkworm silk fibres¹³. **d**, SEM image of the hierarchical Bouligand structure of the dactyl club of the stomatopod¹⁴. **e**, SEM cross-sectional image of natural *Cristaria plicata* nacre with a hierarchical layered microstructure⁹⁰. Scale bars: 50 nm (**a**); 0.5 μm (**b**); 5 μm (**c**); 20 μm (**d**); 1 μm (**e**). Bottom left: synthetic and hybrid composite material morphologies. **f**, AFM image of PVA-coated core-shell clay nanoplatelets³¹. **g**, SEM image of the layered nanostructure of graphene oxide (GO) nanosheets combined with silk fibroin¹⁰¹. **h**, SEM image of artificial hybrid nacre materials comprising laminated clay-biopolymer composite microplatelets with a highly ordered 'brick-and-mortar' arrangement⁹⁰. **i**, AFM image of twisted amyloid fibrillar bundles¹⁵. **j**, SEM image of right-handed helices self-assembled from D-cysteine-stabilized CdTe nanoparticles¹¹⁶. **k**, Optical microscopy image of a hierarchically

organized CNC-polysaccharide composite with periodic helical organization and submicrometre pitch length¹¹⁷. **l**, AFM image of silica-deposited protein core-shell nanofilaments¹¹⁸. **m**, SEM image of nanostructured artificial cellulose nanofibrils with an anisotropic arrangement visible in fractured areas, shown at higher magnification in the inset¹¹⁹. **n**, SEM image of as-spun regenerated silk-CNT fibres, shown at higher magnification in the inset¹²⁰. Scale bars: 1 μm (**f**); 600 nm (**g**); 1 μm (**h**); 100 nm (**i**); 100 nm (**j**); 10 μm (**k**); 50 nm (**l**); 2 μm (**m**); 400 nm (inset of **m**); 20 μm (**n**); 2 μm (inset of **n**). The hierarchical structures translate into global functions (middle) with a range of timescales and characteristic interactions for each order of magnitude (right). Scale bars (shape morphing panel): 5 mm (main); 2.5 mm (inset). Panels adapted with permission from: **b**, ref. ¹¹², American Chemical Society; **i**, ref. ¹¹⁵, RSC; **l**, ref. ¹¹⁸, National Academy of Sciences; **n**, ref. ¹²⁰ under a Creative Commons licence [CC BY 4.0](https://creativecommons.org/licenses/by/4.0/). Panels reproduced with permission from: **c**, ref. ¹¹³, Springer Nature Ltd; **d**, ref. ¹¹⁴, Elsevier; **e**, ref. ⁹⁰ under a Creative Commons licence [CC BY 4.0](https://creativecommons.org/licenses/by/4.0/); **f**, ref. ³¹, Springer Nature Ltd; **h**, ref. ⁹⁰ under a Creative Commons licence [CC BY 4.0](https://creativecommons.org/licenses/by/4.0/); **j**, ref. ¹¹⁶ under a Creative Commons licence [CC BY-NC 4.0](https://creativecommons.org/licenses/by-nc/4.0/); **m**, ref. ¹¹⁹ under a Creative Commons licence [CC BY 4.0](https://creativecommons.org/licenses/by/4.0/); global functions panel, bottom, ref. ²⁰, Springer Nature Ltd.

recreate and programme the complexity of diverse components and interfaces into synthetic processes. Challenges include the combination of different material phases, the creation of composition gradients and reversible energy dissipation with incredible control over local and global mechanics. We will examine the processes through which materials acquire multiple functionalities in the next section.

Synthetic and bioinspired materials

In the following, we survey examples of current state-of-the-art approaches to the design, assembly and understanding of composite materials with elements of hierarchical organization, followed by a global analysis and categorization of mechanical performance relative to traditional composite classes.

Shape-morphing composites with ND functionality

Responsive bioinspired composites are based on the general principles of creating interfacial stresses, with the inclusion of dynamically responsive elements for active transport, self-healing, touch sensors, tunable photonic structures and shape morphing observed in nature (bottom panel in Global Functions and Timescale and interactions in Fig. 2)¹⁷. Volume may change or be conserved in this process, as in sea cucumber (*Holothuroidea*) or Venus flytrap (*Dionaea muscipula*) morphing¹⁸. Hierarchical metamaterials use both active and passive mechanofunctionality in response to external stimuli to achieve ND functionality. Active mechanofunctionality, such as muscles or actions that require energy, corresponds to environmental stimuli responses, such as reversible shape transitions or colour changes. In turn, passive functionality originates from within biological assemblies. Bonds and molecules can rearrange

themselves when exposed to external environmental stimuli while not actively using energy to react. Examples include the sorption-induced bending of wood and the curling of hair in response to heat¹⁹.

One classic example of active bioinspired materials includes dynamic bilayer hydrogels, composed of cellulose fibrils embedded in a soft matrix that enables morphing in wet environments via encoded anisotropic swelling through pre-programmed fibril orientation²⁰. More complex shape transformations (for example, helicoidal) can be achieved by controlling interfacial stresses in the bilayer structures depending on the swelling ratios and elastic moduli. For example, the aspect ratio of silk bilayer nanosheets can control biaxial stresses and self-rolling into different tubular shapes²¹. Engineered structures with pre-programmed elements, sometimes instituted using kirigami or origami, can show organized transformations due to complex buckling and adaptive architectures, and adjust their shapes for complex morphing²². The so-called 4D behaviour with time as an additional axis emphasizes the unique, diverse real-time behaviour of the structures. This direction in research has been explored, for example, in silk-based patches for tympanic membrane repair²³, as well as in soft robotics, which needs special attention beyond the scope of this Review.

Laminated layered composites beyond nacre

Layered bioinspired materials comprising graphitic, cellulosic and other nanomaterials have been produced to mimic and surpass natural nacre composites, in some cases resulting in impressive material performance and functionalities unseen in traditional laminates (Fig. 2f–h)^{16,24,25}. A relatively low volume fraction of reinforcement material in a brick-and-mortar structure can achieve high fracture toughness similar to that of nacre, for example, 3.4 MPa m^{1/2} with 38 wt% clay in polyvinyl alcohol (PVA) composites (comparable to nacre at 4–8 MPa m^{1/2}; Fig. 2f)¹⁵, where PVA increases the composite's energy dissipation. Tougher materials have been designed by alternately stacking microplatelets with similar dimensions to those of aragonite used in nacre between thick chitosan layers^{26,27}. Microplatelets can be decorated with nanoparticles and sintered to adjust the size of asperities and mineral bridges, facilitating resistance to sliding (Fig. 2f–h and top two panels in Global Functions). Engineering of non-platelet functional particles, including hydroxyapatite²⁸ and zirconia polycrystals²⁹, might involve rotation for energy dissipation as a toughening mechanism³⁰.

A strong interface is critical for effective load transfer and energy dissipation, as demonstrated in the early studies using layer-by-layer assembled composites; however, the interface also needs to be compliant to deflect cracks and delocalization stresses. The complementary pairing of polymers with inorganic fillers is characterized by the superposition of multiple types of interfacial interactions that differ in strength and dynamics. Adding polymers to control relaxation dynamics is considered an effective toughening method^{24,31}. Exceptional values of strength and modulus can be achieved in composites with high inorganic phase content (above 90%), contributing to stiffness that increases intrinsic toughening via crack deflection. The necessary interfacial interactions can be tailored via nanosized building blocks during biomineralization^{25,29}. An aspect that has often been overlooked is the biochemistry of proteins, and the surface chemistry of the inorganic platelets or particles, that serve as essential building blocks or templates that accurately regulate biomineralization³². For instance, with recent advances in RNA sequencing and high-throughput proteomics techniques, one can reliably design full-length sequences that have additional reinforcement potential³³.

In another high-performance synthetic nacre, the interlayer polymer is a blend of a chitin–silk fibroin matrix and acidic proteins, which provides a robust interface and a unique interlocking mechanism while facilitating large shear deformation and strain hardening in the polymeric phase³⁴. In this manner, the combination of nanofibrous materials with 2D nanosheets is an efficient option for synergistic strengthening³⁵. A recent breakthrough involves the design of

interfaces that enable large-scale sliding of tablets in engraved glass laminations, leading to up to more than twice the toughness of tempered soda-lime glass and more than three times the toughness of polymethyl methacrylate (PMMA)³⁶. Uniform plate geometry and patterning avoid strain localization and maximize energy dissipation. However, at the next level of hierarchy, additional complexity, such as symmetry-breaking alignment and correlated twisting in stacks, must be introduced to enhance mechanical performance.

Twisted laminated Bouligand and chiral composites

Another class of laminated materials features organized twisted stacking with a slight rotation and twisting angle in adjacent layers, commonly referred to as the Bouligand structure (Fig. 2d)^{37,38}. As seen in mollusc shells and arapaima fish scales in nature, these twisted hierarchical structures demonstrate a remarkable strength and toughness to resist compression and penetration damage³⁹. The unusual toughening mechanism arises from multiple layers in the hierarchical architecture. For example, a mineralization gradient created by a helicoidal arrangement in a herringbone superstructure deflects and twists crack propagation. The striated region consists of circumferentially oriented fibres and exhibits impressive compression during impact and exceptional toughness during stretching⁴⁰. Furthermore, double-Bouligand structures have been found to support mechanical robustness, for example, in the stomatopod dactyl club⁴¹.

These superstructures with unusual performance are a great inspiration for synthetic hierarchical chiral and twisted materials. Various top-down micro- and nanofabrication techniques have been explored, including electrochemical deposition and direct laser writing⁴². Precise control of hierarchical structures from the nanoscale to the macroscale and large-scale fabrication are still a challenge, however. Bottom-up strategies involving the directed assembly of individual entities could provide a faster solution. Better precision at the local level has been achieved by controlling the surface chemistry, geometry and dimensions that enable the fast 'construction' of arbitrary geometries and richer possibilities for integrating additional components (Fig. 2i–k)⁴³. Traditional liquid crystals (LCs) with chiral nematic (cholesteric) phases can be applied as templates, and a well-known example is the organization of polysaccharide nanocrystals, such as cellulose nanocrystals (CNCs) and chitin nanocrystals (ChNCs) derived from plants and crustaceans, respectively, into chiral nematic lyotropic LC phases^{44,45}. Transparent films made from mixtures of wood and CNCs have achieved strengths similar to that of bone¹⁶, and helical organization in CNCs leads to the selective colour reflection of circularly polarized light (Fig. 2k)⁴⁶. Switchable lasers, controlled by relative humidity, have recently been built from plant-based CNCs and fluorescent polymers at room temperature⁴⁷.

In silico studies of the behaviour of the Bouligand shell and thin-film structures have a multitude of mechanisms for coping with mechanical impact⁴¹. Depending on the properties of the fibre material, Bouligand structures can result in bandgaps that promote impact tolerance and facilitate the propagation of deformation waves, resulting in energy redirection and better performance at high strain rates. Experiments demonstrated crack twisting and distributed damage mechanisms with greater energy dissipation due to the minute differences in fibre orientation and reduced delamination. Twisted laminated structures drive the crack path in tortuous trajectories around designed heterogeneities^{39,48}. These examples found in nature are applied in engineered heterogeneous materials, for example, some types of ceramic and ballistic armour. The functionality of Bouligand structures finds uses in optics, acoustics and mechanics; however, current synthetic structural composites are commonly not tough, unlike silks and other fibrous composites.

Fibrous and hairy nanoparticle composites

Fibrous composites are among the most sophisticated hierarchical structures in nature (Figs. 2a, b, l–m and 3). Silk, keratin, cartilage and

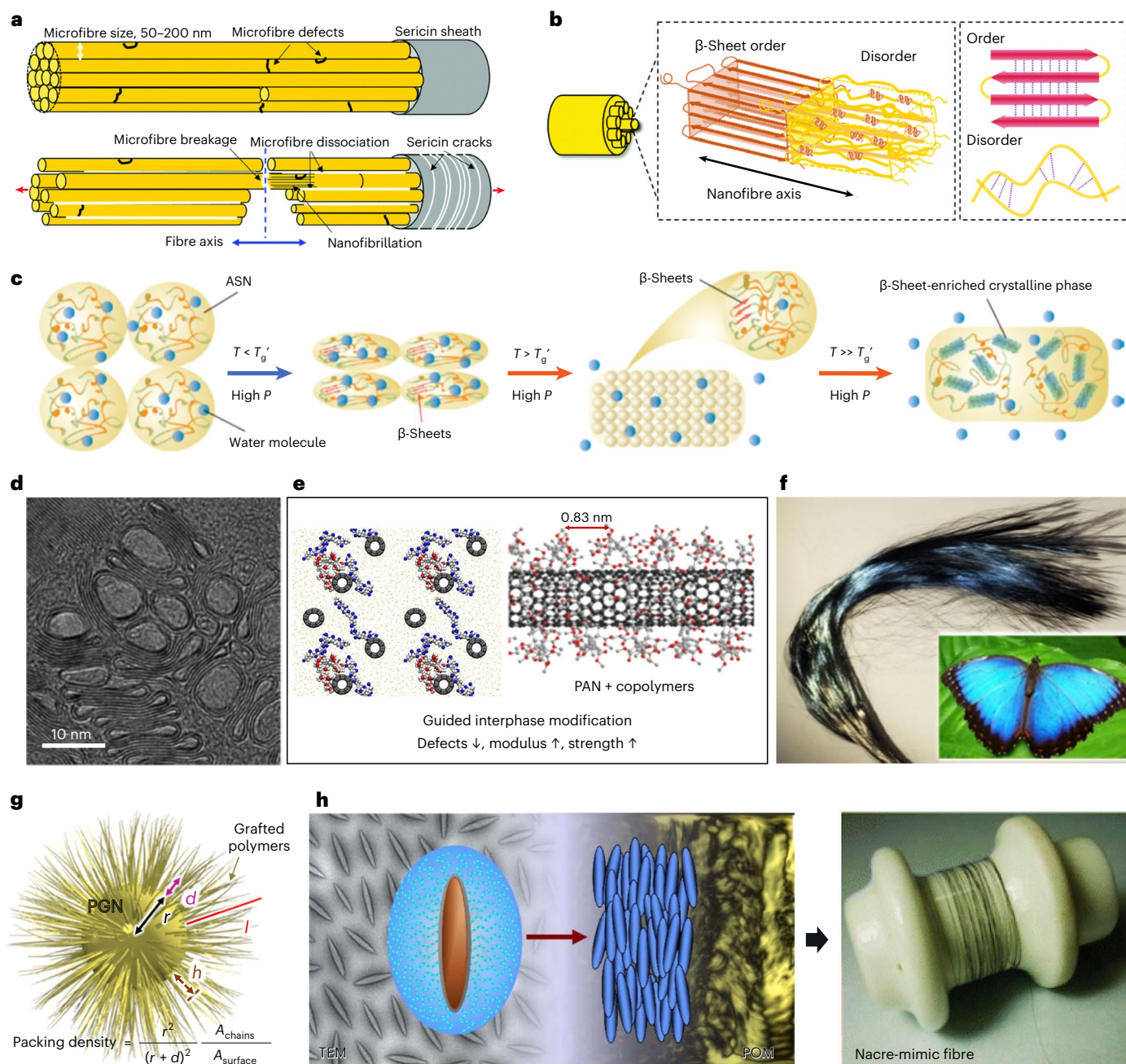


Fig. 3 | Fibre-based composites. **a**, Schematic representations of the microfibrils from *Antheraea pernyi* silk (top) and the deflected fracture path that originates from a crack at the interface between sericin and the silk core (bottom)⁵⁰. **b**, The hierarchical structure of the *A. pernyi* silk fibre. **c**, Proposed mechanism for the structural transition of regenerated amorphous silk nanomaterials (ASNs) during thermal processing under increased pressure (P) of 632 MPa (ref.⁵³). T_g' indicates a water-associated glass transition temperature at 65 °C. **d**, Transmission electron microscopy (TEM) image of CNT-based composites and carbon fibre¹²¹. **e**, Interphase modification by helically ordered wrapping of PMMA and other polymers around single-walled CNTs increases alignment, modulus and strength^{55,56}. **f**, Surface-modified carbon fibres in a polymer matrix demonstrating a blue structural colour⁵⁸. The fibres are the size of human hair. **g**, Scheme of the geometry of polymer-grafted nanoparticles⁶⁰. The packing density of the polymer chains on the particle surface depends on the cross-sectional area of the polymer chains (A_{chains}) relative to the available surface area (A_{surface}). Given a local radius of curvature of the particle r , the packing density of the polymer chains decreases for an increasing distance d from the surface ($d > 0$). The effective thickness of the polymer h is smaller than the extended

chain length l and influences the interfacial properties. The inclusion of solvent and interdigitation with neighbouring nanoparticles controls the toughening mechanism. **h**, An example of the self-assembly of polymer-grafted hairy nanoparticles into fibres. Left: the TEM image shows films of silica-coated α -Fe₂O₃ rods end-grafted with PMMA brushes of ~600 nm length¹²² that self-assemble in a good solvent such as toluene to form lyotropic nematic LCs as seen by polarized optical microscopy (POM). The LC phases are enabled by tight control of the microstructures in PGN-polymer composites and facilitate spinning fibres with control over hierarchical architectures, dramatically enhancing both structural and functional properties. Right: similar processes have been used to graft polyacrylonitrile (PAN) to GO nanoparticles, using a precursor to spin nacre-mimetic fibre¹²³. Two-dimensional materials such as graphene and MXenes¹²⁴, or highly aligned one-dimensional CNTs and CNCs with grafted polymers can also form functional fibres with properties that depend on nanoparticle chemistry and shape. Panels reproduced with permission from: **a, b**, ref.⁵⁰ under a Creative Commons licence CC BY 3.0; **c**, ref.⁵³, Springer Nature Ltd; **d**, ref.¹²¹, Elsevier; **h**, refs.^{122,123}, American Chemical Society. Panel **f** adapted with permission from ref.⁵⁸, American Chemical Society.

basal membranes are examples of an extraordinary class of natural nanomaterials that exhibit unparalleled mechanical performance and additional functionalities, such as ion selectivity, essential for applications in numerous energy technologies^{49–51}. Silks from spiders' webs and cocoons have a wide variety of functions, ranging from the absorption of kinetic energy (spiders' webs) to the protection of larva (hard cocoon), and exhibit increased toughness at high deformation rate⁴⁹ and at cryogenic temperatures⁵⁰. These unique combinations are possible due to the multidomain architecture of silk proteins that controls the energy dissipation mechanisms. Enhanced toughening in silks is governed by the stiffening mechanism of the individual fibrils with increased friction between them, resulting in resistive slippage and diverting crack growth (Fig. 3a)⁵⁰, akin to the morphologies found in carbon nanotube (CNT) fibres⁵². Further toughening mechanisms observed in fibre composites include fibre pull-out and fibre bridging, which contribute to increased fracture toughness. At the molecular level, intrinsic toughening is linked to nanofibrils with a high degree of alignment (Fig. 3b). Furthermore, amorphous silk can convert into highly crystalline silk (Fig. 3c) by processing at temperatures above the glass transition temperature (T_g), resulting in exceptional self-reinforced material properties⁵³. Beyond natural fibres, carbon fibres are examples of ultrastrong and tough materials that exhibit exceptional modulus and strength per unit mass that places them in a special parametric space rarely achieved by other composites (Fig. 3d–f). Their current best performance shows a modulus of ~400 GPa and a tensile strength of ~8 GPa, while the theoretical limits remain at approximately 1,000 and 100 GPa, respectively⁵⁴. Engineering the alignment of CNTs and polymer gel precursors as well as controlling defect formation is necessary to facilitate improvements (Fig. 3d,e)^{55,56}. For example, the precisely tailored interfacial properties of CNT–polymer nanocomposites with PMMA-modified CNTs show an up to fivefold increase in tensile modulus and around a threefold increase in tensile strength⁵⁷. The inhomogeneity of carbon fibre surfaces also causes sp^2 and sp^3 carbon hybridization, which has been exploited to create in situ polymerized hierarchical structures that exhibit structural colour akin to that of butterfly wings (Fig. 3f)^{17,58}.

Polymer-grafted hairy nanoparticles (PGNs) constitute a new generation of synthetic composites (Fig. 3g,h)⁵⁹. PGNs are core–shell particles in which inorganic nanoparticle cores, such as spheres, cubes, cones, rods or sheets, are directly linked to a shell of polymer chains through covalent or non-bonding interactions (panels a–d in Box 1)⁶⁰. These core–shell architectures offer unprecedented opportunities to precision-tailor interphases. The volume fraction of PGNs and the packing density of the grafted polymer chains can be controlled, including as a function of distance from curved nanoparticle surfaces, and entanglements with the polymer matrix control the toughening

mechanism⁶¹. Particles with congruent geometry but having stiff spikes that replicate pollen and viruses also show unusual properties represented by anomalously high resistance against agglomeration and responsive behaviour, as discussed in the next section.

Transcending design across different materials classes

The selected examples of materials designs discussed above do not fully reflect the rich variety of this field. We compare the enormous range of multifunctional attributes and mechanical properties realized in bioinspired composites with traditional engineering composites in the same parametric space in two corresponding Ashby plots (Fig. 4 and Table 1). The analysed composites are colour-coded according to their origin (biological or synthetic materials), type of morphology (nacre-like, twisted, disordered or internal fibrous microstructures) as well as the parametric space occupied by traditional materials classes: ceramics, elastomers, metals and fibrous composites (Fig. 4).

Many engineering materials, such as carbon fibre polymer composites, achieve high strength and stiffness, while aluminium has a lower strength and stiffness but high toughness and ductility³. When analysing the mechanical strength and elasticity (ultimate strength versus ultimate strain) of available materials, which is vital for the practical design of very strong materials with high resilience and non-brittle failure, we observe that known bioinspired composites mostly occupy the same parametric space as traditional composite materials (Fig. 4a). The majority of known bioinspired composites with soft components, such as CNT–silk and PVA–montmorillonite (MTM) clay–nanofibrillated cellulose (NFC) composites, are comparable in ultimate strength to common engineered ceramics, polymers and metals (~0.1–1 GPa; Fig. 4a). The strength of mineral or ceramic components, as well as that of polymers can vary. The softer components, reconfigurable interfaces and gradient organization facilitate greater deformability than synthetic composites, including maximum strains of 10%, and their ability to reconfigure from planar to highly curved or wrinkled structures, resulting in dynamic morphing^{21,59–61}.

The strength of existing biological and bioinspired composites can match advanced synthetic fibre-based composites, for example, when silks, keratins and aramid nanofibres (ANFs) are combined with carbon nanotubes^{14,62}. Beyond the elastic regime, yielding and strain hardening can result from local rearrangements such as disentanglement, strain-induced crystallinity and chain slippage. Such processes add significant plasticity and result in ultimate strains of hundreds of percent. The combination of high ultimate strain with high ultimate strength in some wood–keratin composites sometimes surpasses that reported for synthetic fibrous composites (Fig. 4a). If mechanical performance is considered in terms of toughness versus stiffness (Young's modulus), biological and bioderived composites (that is, those having some quantity of natural materials) also perform like traditional

Fig. 4 | Analysis of the mechanical properties of various composites and comparison with natural and traditional materials classes. a, b, Ashby plots comparing the ultimate strength versus ultimate strain (a) and the toughness versus Young's modulus (b) for various hierarchical biological materials^{14,26,86–88,90}, nacre-mimetic structures^{14,15,26,29,35,89–93,100,125}, Bouligand structures^{48,94–98}, fibre-inspired porous structures^{14,28,62,86,89,99,125}, ordered layered composites and random disordered bionanocomposites^{25,26,87,89,92,99,101–107}. The various strength, strain, toughness (work of fracture) and Young's modulus values were collected from tensile test data. These materials are compared with common materials, shown in light grey, such as engineering metals (stainless steel, gold, copper, silver, tin, nickel, various alloys, titanium, Al and Si carbide, and zinc), engineering polymers (acrylonitrile butadiene styrene, polycarbonate, polyamide, polyether ether ketone, polyethylene, PMMA, polystyrene, polytetrafluoroethylene, polyvinylchloride, POM, polyester, epoxies and polylactic acid), elastomers (butyl rubber, ethylene vinyl, natural rubber, polychloroprene, polyurethane and silicone elastomer), fibres (acrylic, aramid, cellulosic, ultrahigh-molecular-weight polyethylene and polyamide

fibres), carbon fibre/CNTs and CNT composites, engineering ceramics (alumina, aluminium nitride, boron carbide, silicon carbide, silicon nitride, tungsten carbide and zirconia), glasses (borosilicate glass, glass ceramic, silica glass and soda glass) and engineering composites^{108–110}. Hierarchically structured composites achieve the highest combinations of strength and strain, as well as toughness and stiffness. Composites that include biological fibrous components are among the best-performing materials. Hierarchical microstructures imbue unique property combinations via weak and strong interfaces that improve the performance of soft component composites, as established in earlier sections, making them comparable to common inorganic engineering materials. High-end fibre-reinforced composites cannot easily be outperformed in terms of strength and ductility, yet engineering ceramics and metals such as silicon carbide and titanium alloys are outperformed by cellulose nanofibril (CNF)–silk, single-walled CNT (SWCNT)–silk, multiwalled CNT (MWCNT)–silk and Al_2O_3 –chitosan bioinspired composites^{14,26,62}. In these examples, exploiting silk's naturally high strength and ductility while incorporating stiff nanoparticles facilitates an intrinsic toughening mechanism.

composites (Fig. 4b). Bioinspired composites dramatically extend the parametric space towards extremely compliant materials with the unique combination of high toughness and modulus, comparable to that of engineering polymers and ceramics (Fig. 4b). Some of these bioinspired materials occupy valuable, non-traditional parametric space with extreme toughness, up to 100 MJ m^{-3} for silk, chitosan and wood-based composites, as well as high elastic moduli up to tens of gigapascals (Fig. 4b). Bioinspired composites can perform much better than regular elastomers and gels, showing high toughness values up to 10 MJ m^{-3} (Fig. 4b). Specifically, silk- and ANF-based composites

can demonstrate high toughness while not venturing into the standard brittle fracturing regime (Fig. 4b).

Overall, we can conclude that the expansion of characteristics of bioinspired composites into high-performance space with extremes beyond traditional metal and ceramic composites is possible, especially if we consider specific features normalized to material density. However, a deeper understanding of the principles behind hierarchical structural and interfacial organization is required.

In addition, the characterization of hierarchical materials is challenging and benefits from advances in multiple areas that are not

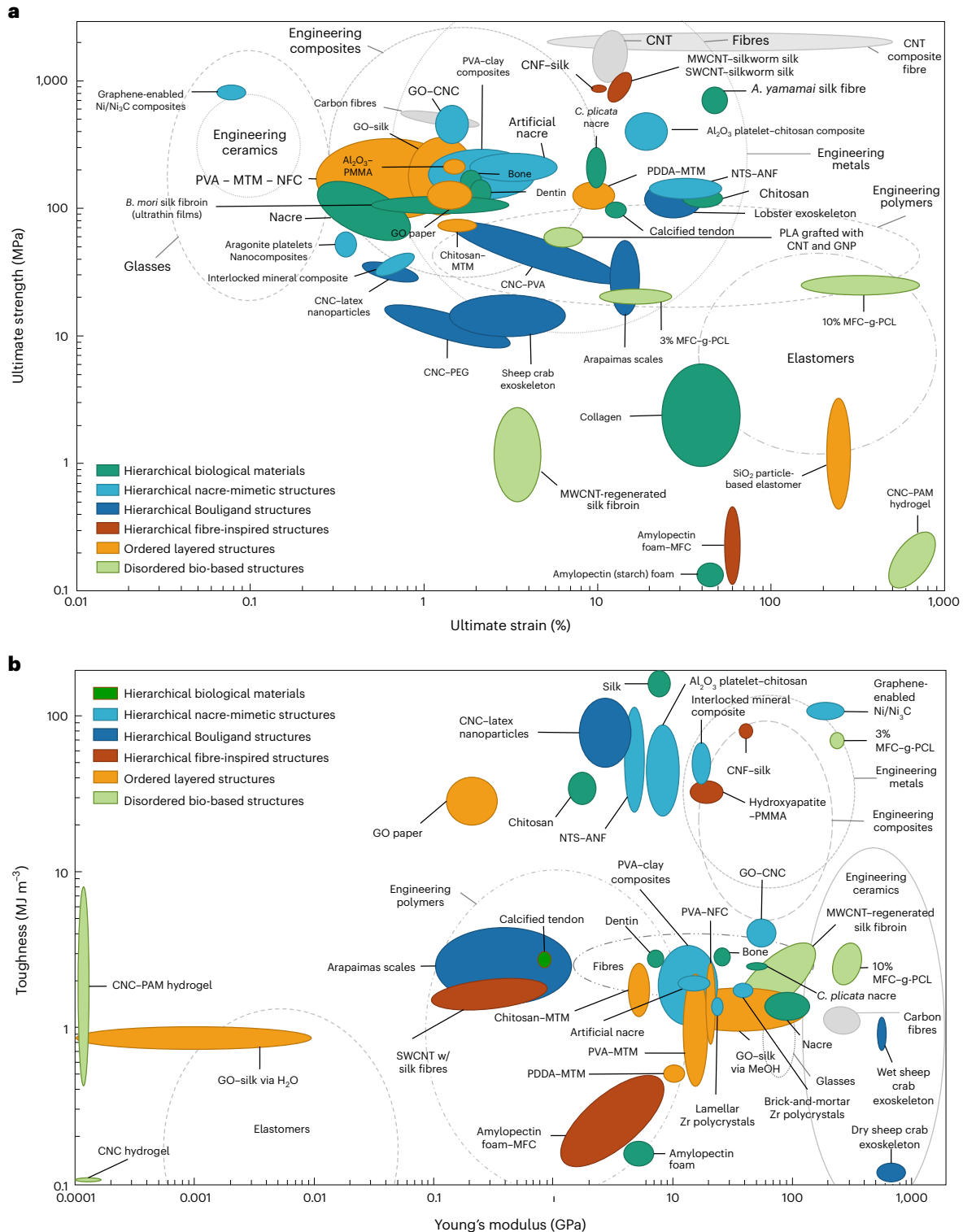


Table 1 | Details of the mechanical properties of the different materials classes

| Material type | Material | Ultimate strength (MPa) | Ultimate strain (%) | Toughness (MJm ⁻³) | Young's modulus (GPa) | Ref. |
|--|--|-------------------------|---------------------|--------------------------------|-----------------------|----------|
| Hierarchical biological | Amylopectin (starch) foam | 0.170±0.025 | -62 | 0.18 | 0.0049±0.0011 | 86 |
| | Bone | 150 | 1.75 | -2.5 | -25 | 26 |
| | Calcified tendon | 80 | 12 | 3.9 | 0.7 | 26 |
| | Chitosan | 108±15 | 42±9 | 32±9 | 1.9±0.3 | 87 |
| | Collagen | 4.2±3.3 | 46±22 | - | 0.025±0.023 | 88 |
| | Dentin | 105 | 2.5 | 2.8 | 7.5 | 26 |
| | Nacre | 95±35 | 0.7±0.5 | 1.8±0.5 | 90±30 | 26,89 |
| | <i>Cristaria plicata</i> nacre | 172±50 | 0.9 | 2.4±0.5 | 49±11 | 90 |
| | <i>Antheraea yamamai</i> silk fibre (silk) | 875 | 35 | -150 | -8.3 | 14 |
| | <i>Bombyx mori</i> silk fibroin | 100±10 | 1.75±1.5 | 0.328 | 7±1 | 88 |
| Hierarchical nacre-mimetic | Al ₂ O ₃ platelet–chitosan composite | 315±95 | 21±5 | 41±19 | 10±2 | 26,89 |
| | Aragonite platelet–organics nanocomposites | 64±8 | 0.38±0.07 | - | - | 14 |
| | Artificial nacre | 267±25 | 4±2 | 2 | 18.6±5 | 90 |
| | Graphene-enabled Ni/Ni ₃ C composite | 1,022±73 | 0.143±0.02 | 110.2±10 | 222±10 | 91 |
| | GO–CNC composite | 490±30 | 1.1±0.3 | 3.9±0.5 | 54±7 | 92 |
| | Planar mineral composite of aragonite films in a chitosan–silk fibroin matrix | 23±2.8 | -0.65 | -8 | -12 | 93 |
| | Interlocked mineral composite of aragonite films in a chitosan–silk fibroin matrix | 43.5±4.5 | -0.9 | -30 | -25 | 93 |
| | Sodium tetrasilic mica–aramid nanofibre composites | 130±15 | 50±24 | 67±33 | 4.7±1.7 | 35 |
| | PVA–MTM clay composites | 170±70 | 2.25±2 | -1.7±0.6 | 17±9 | 15 |
| | Brick-and-mortar Zr polycrystals | - | - | -1.7 | 42±4 | 29 |
| Lamellar Zr polycrystals | - | - | -1.2 | 29±4 | 29 | |
| Hierarchical Bouligand structures | Arapaima scales (dry and hydrated) | -34±17 | -22±14 | -3.6±2.4 | -0.75±0.65 | 48 |
| | CNC–latex nanoparticles | 25±4 | 0.7±0.2 | 0.1±0.02 | 3.5±1.5 | 94 |
| | CNC–polyethylene glycol (PEG) | -13.5±4 | -2.5±2 | - | 1.75±1.25 | 95 |
| | CNC–PVA composites | 57±12 | 3.75±3.25 | - | -7.5±4.5 | 96 |
| | Lobster exoskeleton (dry, in parallel and transverse directions) | -145±35 | -29±16 | - | 4.7±1.6 | 97 |
| | Dry sheep crab exoskeleton | 12.9±1.7 | 1.8 | 0.11 | 764±83 | 98 |
| | Wet sheep crab exoskeleton | 31.5±5.4 | 6.4±1 | 1.02±0.25 | 518±72 | 98 |
| Hierarchical fibre-inspired structures | Amylopectin foam–microfibrillated cellulose (MFC) | 0.7±0.25 | 60±3 | -0.5±0.32 | 0.0046±0.0025 | 86 |
| | CNF–silk composites | 1,050 | 10 | -65 | -35 | 14 |
| | SWCNT–silk fibre composite | 5.5±4 | 2.3±1 | -2.3±1 | 370±300 | 99 |
| | SWCNT–silkworm-spun silk composite | 785±95 | 13.6±1.2 | 6,600±210 | - | 62 |
| | MWCNT–silkworm-spun silk composite | 925±145 | 15.5±1.3 | 9,000±4,500 | - | 62 |
| Ordered layered structures | Al ₂ O ₃ –PMMA (brick-and-mortar) | 200±10 | -1.4 | - | - | 100 |
| | Chitosan–MTM composite | 81±12 | 1.9±0.6 | 0.9±0.4 | 6.1±0.8 | 87 |
| | GO–silk synthesized via H ₂ O | 175±75 | 0.7±0.2 | 0.75±0.25 | 0.005±0.005 | 101 |
| | GO–silk synthesized via MeOH | 225±75 | 1±0.4 | 0.8±1.5 | 75±65 | 101 |
| | GO paper | 113±9 | 0.3±0.16 | 0.25±0.1 | 32±7 | 89 |
| | PDDA–MTM | 100±10 | 10±2 | -0.5 | 11±2 | 25,26,87 |
| | PVA–MTM | 150±40 | 0.7±0.2 | -0.4 | 13±22 | 25 |
| | PVA–MTM crosslinked with glutaraldehyde | 150±40 | 0.33±0.04 | -0.5 | 106±11 | 25 |
| | PVA–NFC | 223±31 | -1.25 | 1.46±0.59 | -15±5 | 102 |
| | PVA–MTM–NFC | 302±12 | -2 | 3.72±0.63 | 22.8±1.0 | 102 |
| | SiO ₂ particle-based elastomer | -2±1.5 | 270±45 | -3±2 | 0.002±0.0015 | 103 |

Table 1 (continued) | Details of the mechanical properties of the different materials classes

| Material type | Material | Ultimate strength (MPa) | Ultimate strain (%) | Toughness (MJ m ⁻³) | Young's modulus (GPa) | Ref. |
|---------------------------------|--------------------------------|-------------------------|---------------------|---------------------------------|-----------------------|---------|
| Disordered bio-based structures | 3% MFC-g-PCL | 20.5±3 | 450±275 | 73±3.3 | 0.245±0.035 | 104 |
| | 10% MFC-g-PCL | 24±4.2 | 20±5 | 2±1 | 0.280±0.075 | 104 |
| | CNC hydrogel | ~0.03 | ~250 | ~0.04 | 0.005 | 105 |
| | CNC-PAM hydrogel | 0.15±0.07 | 716±70 | ~1.6±1 | 0.025±0.007 | 105 |
| | MWCNT-regenerated silk fibroin | ~1.5±1 | ~3.0±0.5 | ~1.9±1.4 | ~0.07±0.05 | 106 |
| | PLA grafted with CNTs and GNP | 66±11 | 6.0±1.1 | – | 2.1±0.5 | 107 |
| Engineering materials | Elastomers | 27±25 | 610±340 | 0.75±0.45 | 0.024±0.02 | 108,109 |
| | Engineering ceramics | 550±450 | 0.12±0.6 | 4.5±3.5 | 700±500 | 108,109 |
| | Engineering composites | 1,050±950 | 5.5±5 | 48±43 | 110±95 | 108,109 |
| | Engineering metals | 1,210±1,000 | 40±39 | 75±65 | 205±190 | 108,109 |
| | Engineering polymers | 60±54 | 401±400 | 5.1±5 | 5.1±5 | 108,109 |
| | Fibres | 2,000±800 | 19±17.5 | 2.5±0.9 | 70±68 | 108,109 |
| | Carbon fibres | 680±40 | 1.4±0.6 | 1.05±0.15 | 45±13 | 109 |
| | CNTs | 1,600±500 | 10±1 | – | – | 109 |
| | CNT composite fibre | 1,800 | 355±345 | – | 80 | 110 |
| | Glasses | 1,000±980 | 0.14±0.10 | 1.0±0.5 | 80±20 | 108,109 |

The table includes the key mechanical properties for different material types, organized into the same groups and colour codes as in the Ashby plots in Fig. 4. The categories are (1) hierarchical biological materials, (2) hierarchical nacre-mimetic materials, (3) hierarchical Bouligand materials, (4) hierarchical fibre-inspired materials, (5) ordered layered materials, (6) disordered bio-based structures that can be used in common hierarchical materials and (7) engineering materials. The data points for individual engineering materials subsets are not detailed here and can be found in the CES EduPack database¹⁰⁹ or the work of Ashby¹⁰⁸. For some materials, the data were not directly reported in the original works and are based on the analysis of tensile data and stress–strain curves using best estimates and error bars. The symbol ‘~’ indicates estimates with high uncertainty. GO paper, GO in the shape of paper-like sheets; PDDA, poly(diallyldimethylammonium); g-PCL, γ -polycaprolactone; PAM, polyacrylamide; GNPs, graphite nanoplatelets.

further reviewed here. Critical techniques include scanning probe microscopy (nano-dynamic mechanical analysis (nano-DMA), AFM–infrared spectroscopy (AFM–IR) and AFM–Raman spectroscopy), high-resolution electron microscopy (high-resolution transmission electron microscopy (HRTEM), scanning transmission electron microscopy (STEM) and electron energy loss spectroscopy (EELS)), synchrotron X-ray and neutron scattering, nano-X-ray computed tomography and advanced spectroscopy, as well as in situ real-time monitoring of mechanical properties and dynamic changes in local chemical and morphological features, under ambient conditions, in fluid environments and at elevated temperatures.

Modelling and simulation of hierarchical materials properties

The modelling and simulation of mechanical and other functional properties can guide the design of bioinspired hierarchical structures within an unlimited space of chemistry and assembly across scales. Simulations typically rely on inputs from experimental data, experimentally inspired data and specific algorithms to calculate sophisticated properties. Knowledge is generated by analysing the computational results and comparison with experimental data, extending material screening to hypothetical model structures and property predictions in iterative feedback loops.

Typically, simulations use individual techniques suitable for specific length scales, while the integration across hierarchies remains difficult (Fig. 2)^{63,32}. Ab initio electronic structure simulations, for example, using density functional theory (DFT), are typically used for a few hundred atoms to investigate geometries, transformations in chemical bonding, cohesive energies, bandgaps and elastic moduli, are limited to picosecond dynamics and exclude electrolytes. As an example, DFT calculations can forecast the strength of crosslinks between fillers and polymer matrices (Fig. 5a)⁶⁴. The information can then be used to assess the mechanical strength of covalently bonded composites via reactive molecular dynamics (MD) simulations and

identify parameters for better reinforcement, such as the diameter of CNTs, the role of defects and suitable polymer chemistries⁶⁵. At the next level, atomistic MD simulations can be used for up to millions of atoms and for dynamics up to microseconds. Performance metrics include the accurate representation of chemical bonding, structure (for example, lattice parameters), surface energies, solvation energies and mechanical properties (see also Box 1)⁶⁶. All-atom MD simulations determined, for example, a reversible actuation of up to 80% for DNA attached to gold nanoparticles, in agreement with experiments on the ~10 nm length scale (Fig. 5b). Structural changes occur in response to the addition of ethanol and a variation in the local dielectric constant⁶⁷, as well as to the addition of multivalent cations that modify the ionic strength⁶⁸. Thermodynamically consistent force fields such as the INTERFACE force field⁶⁶ allow the analysis of inorganic–(bio)organic materials, including binding energies, interfacial shear strengths and glass transition temperatures, with an agreement of about ±5 K with experimental data (Fig. 5c)⁶⁹. The effects of conformation, electrolyte and assembly preference during processing can be monitored in atomic resolution, which is typically not feasible in experiments and supports the design of MD functional bioinspired materials⁵⁵.

Limitations in the size of all-atom models of the order of 100 nm and in the dynamics of the order of 1 μ s can be overcome by coarse-grained (CG) simulations, which sacrifice most chemical detail and can explore 10 to 100 times larger spatial and temporal scales⁶³. CG MD simulations have illuminated the role of interphase regions in nanocomposites (Fig. 5d)⁶¹. In polymer-grafted ‘hairy’ nanoparticles, for instance, a relatively low grafting density and long surfactants were shown to enable significant interdigitation of the modified nanoparticles and improved the mechanical properties (Fig. 5d)^{59,61}. MD and CG methods also uncover scaling relations and provide data to train ML algorithms for accelerated property predictions (Box 2)⁷⁰. At scales beyond micrometres, the mechanical response of composite materials can be effectively analysed using peridynamics simulations, phase field models and the finite element method (FEM)⁷¹. Peridynamics models

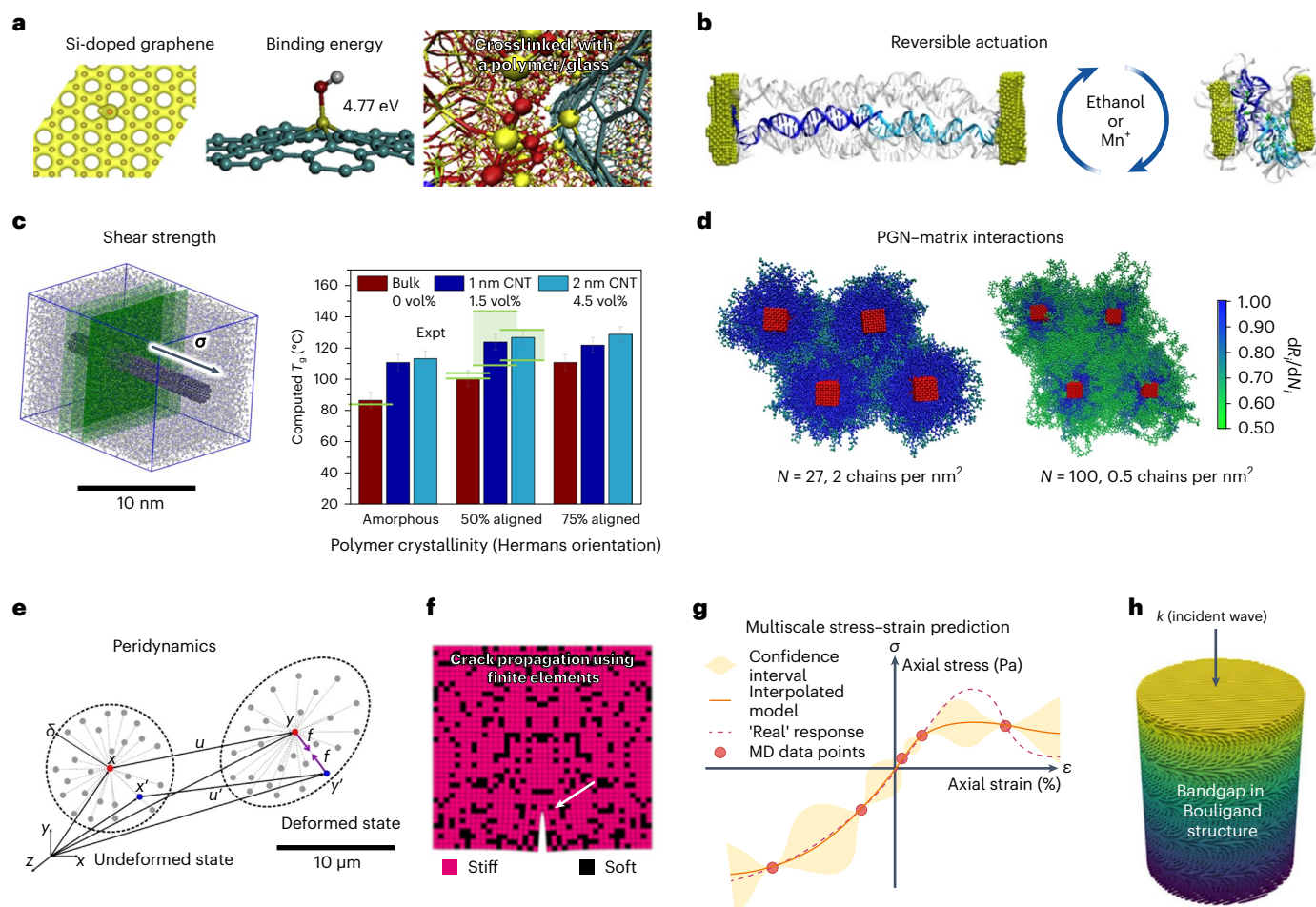


Fig. 5 | Insights into the function and mechanics of bioinspired composites by modelling and simulation. **a**, Electronic structure of local Si defects in graphene and calculation of C–SiH bond energy using DFT. Subsequent all-atom MD simulations of crosslinking on CNT surfaces can guide experiments to optimize bonding to polymer matrices^{64,65}. **b**, Functionalization and up to 80% reversible actuation of gold nanostructures modified with DNA, induced by changes in solvent or ionic concentration according to all-atom MD simulation^{67,68}. **c**, MD simulations of shear strength and glass transitions in PAN–CNT composites. T_g values reveal ± 5 K agreement with experimental data, which are indicated by green shaded error bars where available. The errors bars in each column indicate the statistical uncertainty in the simulation. The molecular origin of T_g and the influence of CNT bundling and volume fraction could be identified⁶⁹. **d**, Hairy nanoparticles support non-covalent mixing with a polymer matrix (green), whereby the packing density and chain length of the ‘hairy surfactants’ (blue) have a critical influence on the composite properties, as shown by coarse-grain MD simulations⁶¹. R_i is the distance of the i th monomer from the nanoparticle surface in Å, and N_i is the monomer position index in the polymer chain. With the advances in reliable all-atom force fields⁶⁶ and larger-scale coarse-grain models⁷¹,

it is possible to predict the role of nano- and microscale features, such as packing, defects and interfaces, on macroscale properties. **e**, In peridynamics, bond lengths and bond failure are monitored to compute continuous deformation and stress–strain characteristics at the microscale. x and x' are the coordinates of two material points before deformation, u and u' are the displacement vectors, and y and y' the new coordinates after deformation. f is the interaction force between the material points y and y' , and δ represents range of interactions between material points (the so-called horizon)⁷³. **f**, Simulation of crack propagation in a FEM simulation (see arrow)⁷⁹. **g**, Results of a multiscale simulation of the mechanical response of a graphene–epoxy composite. From a large set of data points from all-atom simulations and narrowed confidence intervals, Gaussian process regression was used to construct a surrogate continuum model to predict the stress distribution from the current strain for time-independent systems using multiple replicas⁷⁴. **h**, Multiscale simulation of the bandgap in the Bouligand structure of a transversely isotropic material using FEM up to the micrometre scale⁷⁵. Panels reproduced with permission from: **a**, refs. ^{64,65}, Elsevier; **e**, ref. ⁷³, Springer Nature Ltd. Panels adapted with permission from: **b**, ref. ⁶⁷ under a Creative Commons licence [CC BY 3.0](https://creativecommons.org/licenses/by/3.0/); **h**, ref. ⁷⁵, Elsevier.

involve bonds inside the material and mimic associated deformations (Fig. 5e)^{72,73}. Peridynamics is well suited to simulating heterogeneous fracture evolution in polymers, including elastic and plastic deformation, unguided crack nucleation and growth, and crack branching at interfaces. Alternatively, phase-field models can be used that assume a continuum representation and a specific parameter that represents the progress of fracture at every point in the specimen. FEM simulations of fracture can be challenging due to the presence of ubiquitous matrix/inclusion interfaces and complex geometries that defy the underlying continuum assumptions. Atomistically informed FEM simulations can overcome some of these challenges (Fig. 5f,g)⁷⁴ and have been helpful, for example, for analysing crack twisting and distributed damage

mechanisms in Bouligand structures to explain increased energy dissipation before failure and promote impact tolerance⁷⁵. Bandgaps and wave-filtering capabilities could also be identified as a function of the fibre material and orientation (Fig. 5h).

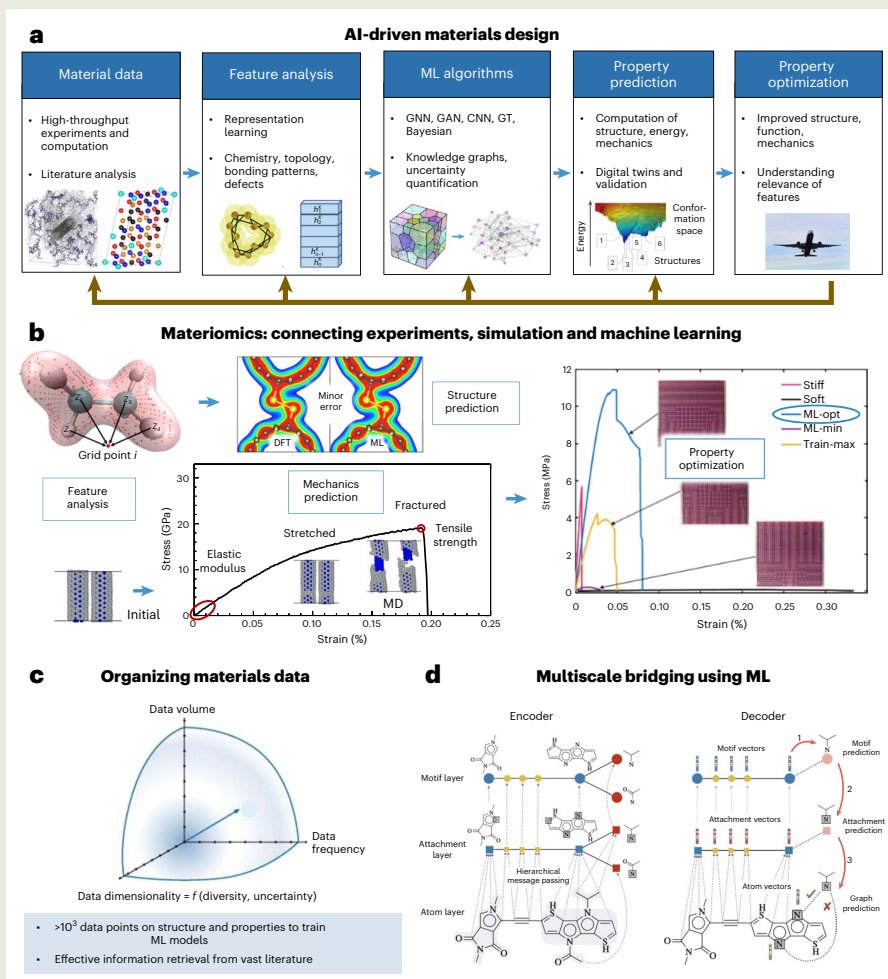
In summary, routine simulations are currently feasible in selected areas on the time–length continuum and provide guidance on specific aspects of composites (Timescale and interactions in Fig. 2). Some methods are also frequently used in combination (MD/DFT, CG/atomistic MD and FEM/MD)^{63,71}. Big challenges include better representation of structure–function phenomena across different length scales and new approaches to predicting the behaviour over long timescales. Fracture mechanisms of bio-based materials are largely an open field as

BOX 2

Future contributions from AI–ML, materiomics and multiscale design

High-throughput experimentation and ML hold great promise to better sample the vast design space (**a**). Generally, large amounts of data for one type of system, from thousands to millions, can be categorized into features and vector representations for ML analysis. Examples of data sources include high volumes of X-ray scattering and spectroscopic data, stacks of images from microscopy and tomography, and data from computational structure–property calculations. Thereby, structural and other physical data elements need to be supplied together with the corresponding physical properties of interest for prediction in the entire dataset, that is, in computer science language, all structural ‘data’ require ‘labels’, to be able to build and train an ML algorithm. The algorithms may involve graph neural networks (GNNs), graph area networks (GANs), convolutional neural networks (CNNs), graph theory (GT) and Bayesian causal discovery. The indices h and k describe the message passing workflow in a GNN. Once trained, the algorithms be applied to predict structural, energetic, mechanical, electronic and other properties for new material structures inside and partially outside the training space. The integration of cutting-edge experimental data into cross-scale simulations and ML facilitates a build–measure–learn feedback

loop to construct interpretable digital platforms (digital twins) for faster property optimization (**b**)^{79,126}. As an example, ML of electronic density features from DFT can be used to predict the atomic-scale structure. ML of data from MD simulations can predict stress–strain curves for carbon-based composites with known defects, allowing recommendation of new designs with increased toughness in a feedback loop with experimental data⁷⁹. The ever-increasing amount of materials data requires tools for systematic organization, considering data volume, frequency of data generation, dimensionality and uncertainties (**c**). Typically, at least thousands of data points are needed to train effective ML models. It is often challenging to retrieve validated information with reliable uncertainties from the rapidly growing number of publications. Hierarchical graph encoders and decoders for molecular structures can be used to accomplish reversible dimensionality reduction when solving multiscale problems by ML (**d**)⁸³. The approaches have promise to overcome the longstanding challenges in multiscale modelling and materials design. Credit (airplane image in **a**): Taras Vyshnya / Alamy Stock Photo. Panel **b** adapted with permission from ref. ⁷⁹, Royal Society of Chemistry; and ref. ¹²⁶, Elsevier. Panel **d** reproduced with permission from ref. ⁸³, PMLR.



they have been far less studied than those of less heterogeneous materials. Specifically, the prediction of tortuous fracture in combined soft and hard material components remains a very challenging problem.

Trends and future developments

Applications of bioinspired composites range from drug delivery, wearable electronics and human–computer interfaces to structural components for the automotive and aerospace industries. The multifunctional attributes imply a unique combination of properties, including mechanical robustness, flexibility, transparency, sensing, adapting (morphing), optics (photonics), as well as electrical and thermal conductivities.

Developing ambient biosynthetic processing techniques

There is a good, albeit still incomplete, understanding of the fundamental building blocks of biological structures. In most cases, it is still not known how nature transitions from the building blocks to the final, complex hierarchical structure, creating a need to better understand the biogenesis or ‘biofabrication’ of materials. There are a few well-studied exceptions, such as the biotechnological production of engineered silk fibres⁷⁶. Recent breakthroughs include understanding of the biofabrication of mussel fibre adhesives⁷⁷ and of the development of complex hard tissues such as the stomatopod dactyl club (Fig. 2d)⁴⁰. However, many intriguing questions remain. For example, the evolutionary principle behind the prevalence of Bouligand structures in biological materials, the structure–mechanical property relationships of the twisting angle and the relative significance of the contribution of material building blocks to the material architecture remain unclear.

Among novel materials design methods, digital manufacturing such as 3D printing combined with advances in AI is rising in prominence due to its ability to create highly complex structures. For example, additive biomanufacturing using silk dopes can preserve natural, sustainable, green and aqueous processes while exploiting new additives, such as aramid nanofibres and other emerging nanofibres from recycled plastics, is vital for the circular economy and adds multifunctionality⁷⁸. Advances in the addition of other polymers, inorganics, sequestration of bioactive components, the use of microfluidic devices for processing, subtle changes in pH and electrolyte composition, as well as sampling the space of processing parameters, offer a suite of new options for 3D printing of hierarchical bioinspired materials. Target properties may include, for example, optical clarity, loading with bioactive components and tunable mechanical performance.

Remarkably, most of the structures discussed here are from natural materials, derived from aqueous-based synthesis and assembly processes conducted at ambient temperature and pressure. When these amazing material outcomes and functional features are considered in the context of using benign conditions to drive material assembly, emulating such systems for our future material needs becomes even more compelling and amplified in importance. New ways to apply environmentally friendly processing with low or negative CO₂ footprint as we move towards the next generation of processing technologies and bioinspired material systems would bring enormous benefits in sustainability to our planet.

Accelerated design using data science and machine learning

Tremendous innovation and acceleration in the precision engineering of nature-inspired materials for targeted functions can be expected by integrating experiments with theory, modelling and simulation, data science and artificial intelligence tools (panel a in Box 2)⁷⁹. While structural order at specific length scales has been experimentally demonstrated in synthetic composites, structural hierarchy across multiple length scales is still lacking and may be achieved more quickly using such convergent techniques. Simulation and data-driven methods, complemented by mathematical approaches such as category theory, can link the physical-chemical properties, characteristics and function

of a material. The synergy of these approaches has led to the new field of materiomics, which aims to order in a unified manner the vast materials space and to accelerate materials design (panels b and c in Box 2)^{32,70}.

Specifically, ML algorithms can accelerate materials discovery as follows⁷⁹. Large training sets of data using features of the electronic, atomic or microscopic scale and known mechanical and other physical properties can be used to train neural networks such as graph neural networks (GNNs) and convolutional neural networks (CNNs) for learning and connecting structure–property relationships⁸⁰. The models are then suitable to make property predictions for untested structures and help to optimize synthesis and design (panels a and b in Box 2). Opportunities in materials design are also emerging using graph theory (GT)-based descriptions of nanocomposites, which can capture the network structure of nanofibre reinforcements⁸¹. Concepts from visual art and music have been combined with AI to navigate the vast space of protein sequences⁸². The rapidly growing amount of data from high-throughput experiments and simulations benefits from the organization in databases with consistent and statistically robust content and multidimensional analysis (panel c in Box 2). A bottleneck is often the extraction of relevant data for a given problem from the literature, which may involve thousands of publications and could be accelerated by advances in information retrieval and natural language processing.

Data science also provides tools to better connect high-fidelity modelling and simulation across different scales. Specific chemistry knowledge has been precisely translated into all-atom models and force fields to carry out predictive MD simulations^{32,66}. Nevertheless, coverage of a diverse range of materials chemistry and the integrated simulation of deformation and fracture behaviour from the atomic scale to the macroscale remains a great challenge. Obstacles involve (1) quickly and accurately parameterizing new chemistry and (2) effectively passing information from atomistic models to CG models and continuum representations. In addition, uncertainties in the experimental nanoscale mechanical characterization of soft materials add barriers to providing guidance and validation for modelling. Data science and machine learning methods are promising to perform the necessary dimensionality reductions of structures and interaction energies between particles and domains upon entering larger scales (panel d in Box 2)⁸³. Such tasks may be achieved in uniform ways by using hierarchical graph encoders and decoders, where chemical identity, geometry and topological patterns play a critical role, similar to those explored earlier for multiscale simulations in adaptive resolution⁶³. ML techniques can also be adjusted to enforce certain principles such as a Hamiltonian system if used to substitute physics-based simulations. Community-wide efforts to standardize reference states, key properties for validation, protocols for simulations and documentation of ML algorithms would enhance reproducible usage and integration of computational and experimental methods.

Future trends and impact

Nature is highly efficient in designing materials with unique optical, mechanical and other functional property combinations through distinctive processing techniques. The integration of experimental and theoretical work can uncover new classes of bioinspired materials that impact society enormously through a unique amalgamation of properties. Modelling techniques, including multiscale simulation, AI and ML, and materiomics, may reveal hidden opportunities for designing multifunctional materials with high strength and toughness at faster development rates through sustainable routes, increasing the efficiency of materials design. However, challenges remain in fulfilling the demand of these bioinspired composites in high-performance applications such as aerospace composites, where extreme temperature, pressure and mechanical tolerance are prerequisites. Multiple other functional attributes, such as electrical conductivity, optical transparency, morphing and self-repair, could be necessary along with

the structural attributes. So far, the incorporation of nanofillers with precisely tailored interfaces into bioinspired hierarchical designs has shown promise and there is an enormous opportunity for innovation⁸⁴.

Similarly, bioinspired composites are a treasure for other fields such as biomedical implants and sensors via grafts and engineering, energy storage via lightweight batteries, global sustainability via ambient processing and self-repair, and communication and coding via adaptivity and hidden functionalities. In addition, the ambient assembly processes reveal important lessons to emulate in the broader context of materials recycling and upcycling.

Recent developments in laser-grade bioinspired photonic band-gap materials also showcase the potential for unprecedented applications beyond physical structures, such as optical communication and adaptive camouflaging⁴⁷. The insights from bioinspired cross-platform approaches answer practically relevant questions such as the high strength of silk, the emergence of disease, the creation of new materials and the underpinning philosophy of what constitutes a material. The integration of insights at different structural levels of hierarchy poses a new paradigm for elucidating the fundamental biogenic fabrication processes and emergence of advanced properties in materials. Therefore, a new horizon of engineered living materials features unique opportunities to create intelligent systems on demand, by combining nature and synthetic analogues to create self-organizing, self-powered, self-sustained and self-evolving structures⁸⁵.

References

- Wegst, U. G. K., Bai, H., Saiz, E., Tomsia, A. P. & Ritchie, R. O. Bioinspired structural materials. *Nat. Mater.* **14**, 23–36 (2015).
- Liu, Z. Q., Meyers, M. A., Zhang, Z. F. & Ritchie, R. O. Functional gradients and heterogeneities in biological materials: design principles, functions, and bioinspired applications. *Prog. Mater. Sci.* **88**, 467–498 (2017).
- Clancy, A. J., Anthony, D. B. & De Luca, F. Metal mimics: lightweight, strong, and tough nanocomposites and nanomaterial assemblies. *ACS Appl. Mater. Interfaces* **12**, 15955–15975 (2020).
- Ritchie, R. O. The conflicts between strength and toughness. *Nat. Mater.* **10**, 817–822 (2011).
- Kotov, N. A., Dekany, I. & Fendler, J. H. Ultrathin graphite oxide–polyelectrolyte composites prepared by self-assembly: transition between conductive and non-conductive states. *Adv. Mater.* **8**, 637–641 (1996).
- Huang, W. et al. Multiscale toughening mechanisms in biological materials and bioinspired designs. *Adv. Mater.* **31**, 1901561 (2019).
- Tadepalli, S., Slocik, J. M., Gupta, M. K., Naik, R. R. & Singamaneni, S. Bio-optics and bio-inspired optical materials. *Chem. Rev.* **117**, 12705–12763 (2017).
- Wang, B., Yang, W., McKittrick, J. & Meyers, M. A. Keratin: structure, mechanical properties, occurrence in biological organisms, and efforts at bioinspiration. *Prog. Mater. Sci.* **76**, 229–318 (2016).
- Huang, W. et al. A natural energy absorbent polymer composite: the equine hoof wall. *Acta Biomater.* **90**, 267–277 (2019).
- Chen, M. L. et al. The hierarchical structure and mechanical performance of a natural nanocomposite material: the turtle shell. *Colloids Surf. A* **520**, 97–104 (2017).
- Hieronymus, T. L., Witmer, L. M. & Ridgely, R. C. Structure of white rhinoceros (*Ceratotherium simum*) horn investigated by X-ray computed tomography and histology with implications for growth and external form. *J. Morphol.* **267**, 1172–1176 (2006).
- Chon, M. J. et al. Lamellae spatial distribution modulates fracture behavior and toughness of African pangolin scales. *J. Mech. Behav. Biomed. Mater.* **76**, 30–37 (2017).
- Teyssier, J., Saenko, S. V., van der Marel, D. & Milinkovitch, M. C. Photonic crystals cause active colour change in chameleons. *Nat. Commun.* **6**, 6368 (2015).
- Ren, J. et al. Biological material interfaces as inspiration for mechanical and optical material designs. *Chem. Rev.* **119**, 12279–12336 (2019).
- Morits, M. et al. Toughness and fracture properties in nacre-mimetic clay/polymer nanocomposites. *Adv. Funct. Mater.* **27**, 1605378 (2017).
- Natarajan, B. & Gilman, J. Bioinspired bouligand cellulose nanocrystal composites: a review of mechanical properties. *Phil. Trans. A* **376**, 20170050 (2018).
- Zhao, Q. L., Wang, Y. L., Cui, H. Q. & Du, X. M. Bio-inspired sensing and actuating materials. *J. Mater. Chem. C* **7**, 6493–6511 (2019).
- de Espinosa, L. M., Meesorn, W., Moatsou, D. & Weder, C. Bioinspired polymer systems with stimuli-responsive mechanical properties. *Chem. Rev.* **117**, 12851–12892 (2017).
- Egan, P., Sinko, R., LeDuc, P. R. & Keten, S. The role of mechanics in biological and bio-inspired systems. *Nat. Commun.* **6**, 7418 (2015).
- Gladman, A. S., Matsumoto, E. A., Nuzzo, R. G., Mahadevan, L. & Lewis, J. A. Biomimetic 4D printing. *Nat. Mater.* **15**, 413–418 (2016).
- Ye, C. H. et al. Bimorph silk microsheets with programmable actuating behavior: experimental analysis and computer simulations. *ACS Appl. Mater. Interfaces* **8**, 17694–17706 (2016).
- Zhang, Y. H. et al. A mechanically driven form of Kirigami as a route to 3D mesostructures in micro/nanomembranes. *Proc. Natl Acad. Sci. USA* **112**, 11757–11764 (2015).
- Lee, J. H., Lee, J. S., Kim, D. K., Park, C. H. & Lee, H. R. Clinical outcomes of silk patch in acute tympanic membrane perforation. *Clin. Exp. Otorhinolaryngol.* **8**, 117–122 (2015).
- Zhao, C. et al. Layered nanocomposites by shear-flow-induced alignment of nanosheets. *Nature* **580**, 210–215 (2020).
- Podsiadlo, P. et al. Ultrastrong and stiff layered polymer nanocomposites. *Science* **318**, 80–83 (2007).
- Bonderer, L. J., Studart, A. R. & Gauckler, L. J. Bioinspired design and assembly of platelet reinforced polymer films. *Science* **319**, 1069–1073 (2008).
- Grossman, M. et al. Mineral nano-interconnectivity stiffens and toughens nacre-like composite materials. *Adv. Mater.* **29**, 1605039 (2017).
- Bai, H. et al. Bioinspired hydroxyapatite/poly(methyl methacrylate) composite with a nacre-mimetic architecture by a bidirectional freezing method. *Adv. Mater.* **28**, 50–56 (2016).
- Tan, G. Q. et al. Nature-inspired nacre-like composites combining human tooth-matching elasticity and hardness with exceptional damage tolerance. *Adv. Mater.* **31**, 1904603 (2019).
- Mao, L. B. et al. Synthetic nacre by predesigned matrix-directed mineralization. *Science* **354**, 107–110 (2016).
- Das, P. et al. Nacre-mimetics with synthetic nanoclays up to ultrahigh aspect ratios. *Nat. Commun.* **6**, 5967 (2015).
- Heinz, H. & Ramezani-Dakhel, H. Simulations of inorganic–bioorganic interfaces to discover new materials: insights, comparisons to experiment, challenges, and opportunities. *Chem. Soc. Rev.* **45**, 412–448 (2016).
- Tan, Y. P. et al. Infiltration of chitin by protein coacervates defines the squid beak mechanical gradient. *Nat. Chem. Biol.* **11**, 488–495 (2015).
- Gim, J. et al. Nanoscale deformation mechanics reveal resilience in nacre of *Pinna nobilis* shell. *Nat. Commun.* **10**, 4822 (2019).
- Zeng, F. Z. et al. A bioinspired ultratough multifunctional mica-based nanopaper with 3D aramid nanofiber framework as an electrical insulating material. *ACS Nano* **14**, 611–619 (2020).
- Yin, Z., Hannard, F. & Barthelat, F. Impact-resistant nacre-like transparent materials. *Science* **364**, 1260–1263 (2019).
- Weaver, J. C. et al. The stomatopod dactyl club: a formidable damage-tolerant biological hammer. *Science* **336**, 1275–1280 (2012).

38. Grunenfelder, L. K. et al. Bio-inspired impact-resistant composites. *Acta Biomater.* **10**, 3997–4008 (2014).
39. Yang, W. et al. Protective role of *Arapaima gigas* fish scales: structure and mechanical behavior. *Acta Biomater.* **10**, 3599–3614 (2014).
40. Huang, W. et al. A natural impact-resistant bicontinuous composite nanoparticle coating. *Nat. Mater.* **19**, 1236–1243 (2020).
41. Yaraghi, N. A. et al. A sinusoidally architected helicoidal biocomposite. *Adv. Mater.* **28**, 6835–6844 (2016).
42. Gansel, J. K. et al. Gold helix photonic metamaterial as broadband circular polarizer. *Science* **325**, 1513–1515 (2009).
43. Urban, M. J. et al. Chiral plasmonic nanostructures enabled by bottom-up approaches. *Annu. Rev. Phys. Chem.* **70**, 275–299 (2019).
44. Ling, S. J., Kaplan, D. L. & Buehler, M. J. Nanofibrils in nature and materials engineering. *Nat. Rev. Mater.* **3**, 18016 (2018).
45. Nikolov, S. et al. Revealing the design principles of high-performance biological composites using ab initio and multiscale simulations: the example of lobster cuticle. *Adv. Mater.* **22**, 519–526 (2010).
46. Cherpak, V. et al. Robust chiral organization of cellulose nanocrystals in capillary confinement. *Nano Lett.* **18**, 6770–6777 (2018).
47. Guo, J. Q. et al. Biodegradable laser arrays self-assembled from plant resources. *Adv. Mater.* **32**, 2002332 (2020).
48. Lin, Y. S., Wei, C. T., Olevsky, E. A. & Meyers, M. A. Mechanical properties and the laminate structure of *Arapaima gigas* scales. *J. Mech. Behav. Biomed. Mater.* **4**, 1145–1156 (2011).
49. Yazawa, K., Malay, A. D., Masunaga, H., Norma-Rashid, Y. & Numata, K. Simultaneous effect of strain rate and humidity on the structure and mechanical behavior of spider silk. *Commun. Mater.* **1**, 10 (2020).
50. Fu, C. J. et al. Cryogenic toughness of natural silk and a proposed structure–function relationship. *Mater. Chem. Front.* **3**, 2507–2513 (2019).
51. Tung, S. O., Ho, S., Yang, M., Zhang, R. L. & Kotov, N. A. A dendrite-suppressing composite ion conductor from aramid nanofibres. *Nat. Commun.* **6**, 6152 (2015).
52. Gupta, N., Alred, J. M., Penev, E. S. & Yakobson, B. I. Universal strength scaling in carbon nanotube bundles with frictional load transfer. *ACS Nano* **15**, 1342–1350 (2021).
53. Guo, C. C. et al. Thermoplastic moulding of regenerated silk. *Nat. Mater.* **19**, 102–108 (2020).
54. Chang, H., Luo, J., Gulgunje, P. V. & Kumar, S. Structural and functional fibers. *Ann. Rev. Mater. Res.* **47**, 1–13.29 (2017).
55. Pramanik, C., Gissinger, J. R., Kumar, S. & Heinz, H. Carbon nanotube dispersion in solvents and polymer solutions: mechanisms, assembly, and preferences. *ACS Nano* **11**, 12805–12816 (2017).
56. Davijani, A. A. B. & Kumar, S. Ordered wrapping of poly(methyl methacrylate) on single wall carbon nanotubes. *Polymer* **70**, 278–281 (2015).
57. Bakhtiary Davijani, A. A., Chang, H., Liu, H. C., Luo, J. & Kumar, S. Stress transfer in nanocomposites enabled by poly(methyl methacrylate) wrapping of carbon nanotubes. *Polymer* **130**, 191–198 (2017).
58. Eyckens, D. J. et al. Fiber with butterfly wings: creating colored carbon fibers with increased strength, adhesion, and reversible malleability. *ACS Appl. Mater. Interfaces* **11**, 41617–41625 (2019).
59. Asai, M., Zhao, D. & Kumar, S. K. Role of grafting mechanism on the polymer coverage and self-assembly of hairy nanoparticles. *ACS Nano* **11**, 7028–7035 (2017).
60. Heinz, H. et al. Nanoparticle decoration with surfactants: molecular interactions, assembly, and applications. *Surf. Sci. Rep.* **72**, 1–58 (2017).
61. Hansoge, N. K. et al. Materials by design for stiff and tough hairy nanoparticle assemblies. *ACS Nano* **12**, 7946–7958 (2018).
62. Xu, H. et al. Obtaining high mechanical performance silk fibers by feeding purified carbon nanotube/lignosulfonate composite to silkworms. *RSC Adv.* **9**, 3558–3569 (2019).
63. Praprotnik, M., Site, L. D. & Kremer, K. Multiscale simulation of soft matter: from scale bridging to adaptive resolution. *Annu. Rev. Phys. Chem.* **59**, 545–571 (2008).
64. Lu, J. X., Luo, M. & Yakobson, B. I. Glass composites reinforced with silicon-doped carbon nanotubes. *Carbon* **128**, 231–236 (2018).
65. Tsafack, T. et al. Exploring the interface between single-walled carbon nanotubes and epoxy resin. *Carbon* **105**, 600–606 (2016).
66. Heinz, H., Lin, T.-J., Mishra, R. K. & Emami, F. S. Thermodynamically consistent force fields for the assembly of inorganic, organic, and biological nanostructures: the INTERFACE force field. *Langmuir* **29**, 1754–1765 (2013).
67. Mason, J. A. et al. Contraction and expansion of stimuli-responsive DNA bonds in flexible colloidal crystals. *J. Am. Chem. Soc.* **138**, 8722–8725 (2016).
68. Samanta, D. et al. Multivalent cation-induced actuation of DNA-mediated colloidal superlattices. *J. Am. Chem. Soc.* **141**, 19973–19977 (2019).
69. Gissinger, J. R., Pramanik, C., Newcomb, B., Kumar, S. & Heinz, H. Nanoscale structure–property relationships of polyacrylonitrile/CNT composites as a function of polymer crystallinity and CNT diameter. *ACS Appl. Mater. Interfaces* **10**, 1017–1027 (2018).
70. Zhao, H. et al. NanoMine schema: an extensible data representation for polymer nanocomposites. *APL Mater.* **6**, 111108 (2018).
71. Gooneie, A., Schuschnigg, S. & Holzer, C. A review of multiscale computational methods in polymeric materials. *Polymers* **9**, 16 (2017).
72. Ha, Y. & Bobaru, F. Studies of dynamic crack propagation and crack branching with peridynamics. *Int. J. Fract.* **162**, 229–244 (2010).
73. Wang, B., Oterkus, S. & Oterkus, E. Determination of horizon size in state-based peridynamics. *Continuum Mech. Thermodyn.* <https://doi.org/10.1007/s00161-020-00896-y> (2020).
74. Vassaux, M., Sinclair, R. C., Richardson, R. A., Suter, J. L. & Coveney, P. V. The role of graphene in enhancing the material properties of thermosetting polymers. *Adv. Theory Simul.* **2**, 1800168 (2019).
75. Guarín-Zapata, N., Gomez, J., Kisailus, D. & Zavattieri, P. D. Bandgap tuning in bioinspired helicoidal composites. *J. Mech. Phys. Solids* **131**, 344–357 (2019).
76. Kronqvist, N. et al. Efficient protein production inspired by how spiders make silk. *Nat. Commun.* **8**, 15504 (2017).
77. Valois, E., Mirshafian, R. & Waite, J. H. Phase-dependent redox insulation in mussel adhesion. *Sci. Adv.* **6**, eaaz6486 (2020).
78. Wang, C. Y., Xia, K. L., Zhang, Y. Y. & Kaplan, D. L. Silk-based advanced materials for soft electronics. *Acc. Chem. Res.* **52**, 2916–2927 (2019).
79. Gu, G. X., Chen, C. T., Richmond, D. J. & Buehler, M. J. Bioinspired hierarchical composite design using machine learning: simulation, additive manufacturing, and experiment. *Mater. Horiz.* **5**, 939–945 (2018).
80. Wu, Z. et al. A comprehensive survey on graph neural networks. *IEEE Trans. Neural Netw. Learn. Syst.* **32**, 4–24 (2021).
81. Wang, M. Q. et al. Biomimetic structural batteries for robotics. *Sci. Robot.* **5**, eaba1912 (2020).
82. Yu, C. H., Qin, Z., Martín-Martínez, F. J. & Buehler, M. J. A self-consistent sonification method to translate amino acid sequences into musical compositions and application in protein design using artificial intelligence. *ACS Nano* **13**, 7471–7482 (2019).

83. Jin, W., Barzilay, R. & Jaakkola, T. Hierarchical generation of molecular graphs using structural motifs. In *Proc. 37th International Conference on Machine Learning* (eds Hal, D. III & Aarti, S.) 119, 4839–4848 (PMLR, 2020).
84. Lossada, F., Jiao, D., Hoenders, D. & Walther, A. Recyclable and light-adaptive vitrimer-based nacre-mimetic nanocomposites. *ACS Nano* **15**, 5043–5055 (2021).
85. Xin, A. et al. Growing living composites with ordered microstructures and exceptional mechanical properties. *Adv. Mater.* **33**, 2006946 (2021).
86. Svagan, A. J., Samir, M. A. S. A. & Berglund, L. A. Biomimetic foams of high mechanical performance based on nanostructured cell walls reinforced by native cellulose nanofibrils. *Adv. Mater.* **20**, 1263–1269 (2008).
87. Podsiadlo, P., Tang, Z., Shim, B. S. & Kotov, N. A. Counterintuitive effect of molecular strength and role of molecular rigidity on mechanical properties of layer-by-layer assembled nanocomposites. *Nano Lett.* **7**, 1224–1231 (2007).
88. Jiang, C. et al. Mechanical properties of robust ultrathin silk fibroin films. *Adv. Funct. Mater.* **17**, 2229–2237 (2007).
89. Cheng, Q., Jiang, L. & Tang, Z. Bioinspired layered materials with superior mechanical performance. *Acc. Chem. Res.* **47**, 1256–1266 (2014).
90. Gao, H. L. et al. Mass production of bulk artificial nacre with excellent mechanical properties. *Nat. Commun.* **8**, 287 (2017).
91. Zhang, Y. et al. Bioinspired, graphene-enabled Ni composites with high strength and toughness. *Sci. Adv.* **5**, eaav5577 (2019).
92. Xiong, R. et al. Ultrarobust transparent cellulose nanocrystal-graphene membranes with high electrical conductivity. *Adv. Mater.* **28**, 1501–1509 (2016).
93. Raut, H. K. et al. Tough and strong: cross-lamella design imparts multifunctionality to biomimetic nacre. *ACS Nano* **14**, 9771–9779 (2020).
94. Vollick, B., Kuo, P. Y., Therien-Aubin, H., Yan, N. & Kumacheva, E. Composite cholesteric nanocellulose films with enhanced mechanical properties. *Chem. Mater.* **29**, 789–795 (2017).
95. Gu, M., Jiang, C., Liu, D., Prempeh, N. & Smalyukh, I. I. Cellulose nanocrystal/poly(ethylene glycol) composite as an iridescent coating on polymer substrates: structure-color and interface adhesion. *ACS Appl. Mater. Interfaces* **8**, 32565–32573 (2016).
96. Wang, B. & Walther, A. Self-assembled, iridescent, crustacean-mimetic nanocomposites with tailored periodicity and layered cuticular structure. *ACS Nano* **9**, 10637–10646 (2015).
97. Sachs, C., Fabritius, H. & Raabe, D. Influence of microstructure on deformation anisotropy of mineralized cuticle from the lobster *Homarus americanus*. *J. Struct. Biol.* **161**, 120–132 (2008).
98. Chen, P.-Y., Lin, A. Y.-M., McKittrick, J. & Meyers, M. A. Structure and mechanical properties of crab exoskeletons. *Acta Biomater.* **4**, 587–596 (2008).
99. Ayutsede, J. et al. Carbon nanotube reinforced *Bombyx mori* silk nanofibers by the electrospinning process. *Biomacromolecules* **7**, 208–214 (2006).
100. Munch, E. et al. Tough, bio-inspired hybrid materials. *Science* **322**, 1516–1520 (2008).
101. Hu, K., Gupta, M. K., Kulkarni, D. D. & Tsukruk, V. V. Ultra-robust graphene oxide-silk fibroin nanocomposite membranes. *Adv. Mater.* **25**, 2301–2307 (2013).
102. Wang, J., Cheng, Q., Lin, L. & Jiang, L. Synergistic toughening of bioinspired poly(vinyl alcohol)-clay-nanofibrillar cellulose artificial nacre. *ACS Nano* **8**, 2739–2745 (2014).
103. Watanabe, K. et al. Highly transparent and tough filler composite elastomer inspired by the cornea. *ACS Mater. Lett.* **2**, 325–330 (2020).
104. Lönnberg, H., Larsson, K., Lindström, T., Hult, A. & Malmström, E. Synthesis of polycaprolactone-grafted microfibrillated cellulose for use in novel bionanocomposites—influence of the graft length on the mechanical properties. *ACS Appl. Mater. Interfaces* **3**, 1426–1433 (2011).
105. Yang, J., Han, C.-R., Zhang, X.-M., Xu, F. & Sun, R.-C. Cellulose nanocrystals mechanical reinforcement in composite hydrogels with multiple cross-links: correlations between dissipation properties and deformation mechanisms. *Macromolecules* **47**, 4077–4086 (2014).
106. Pan, H. et al. Significantly reinforced composite fibers electrospun from silk fibroin/carbon nanotube aqueous solutions. *Biomacromolecules* **13**, 2859–2867 (2012).
107. Scaffaro, R. & Maio, A. Integrated ternary bionanocomposites with superior mechanical performance via the synergistic role of graphene and plasma treated carbon nanotubes. *Composites B* **168**, 550–559 (2019).
108. Ashby, M. F. Overview no. 80: on the engineering properties of materials. *Acta Metall.* **37**, 1273–1293 (1989).
109. *CES EduPack* (Granta Design, 2009).
110. Dalton, A. B. et al. Super-tough carbon-nanotube fibres—these extraordinary composite fibres can be woven into electronic textiles. *Nature* **423**, 703–703 (2003).
111. Grant, A. M. et al. Silk fibroin–substrate interactions at heterogeneous nanocomposite interfaces. *Adv. Funct. Mater.* **26**, 6380–6392 (2016).
112. Wang, Q. et al. Observations of 3 nm silk nanofibrils exfoliated from natural silkworm silk fibers. *ACS Mater. Lett.* **2**, 153–160 (2020).
113. Shao, Z. Z. & Vollrath, F. Surprising strength of silkworm silk. *Nature* **418**, 741 (2002).
114. Guarín-Zapata, N., Gomez, J., Yaraghi, N., Kisailus, D. & Zavattieri, P. D. Shear wave filtering in naturally-occurring Bouligand structures. *Acta Biomater.* **23**, 11–20 (2015).
115. Adamcik, J. et al. Measurement of intrinsic properties of amyloid fibrils by the peak force QNM method. *Nanoscale* **4**, 4426–4429 (2012).
116. Feng, W. C. et al. Assembly of mesoscale helices with near-unity enantiomeric excess and light–matter interactions for chiral semiconductors. *Sci. Adv.* **3**, e1601159 (2017).
117. Adstedt, K. et al. Chiral cellulose nanocrystals with intercalated amorphous polysaccharides for controlled iridescence and enhanced mechanics. *Adv. Funct. Mater.* **30**, 2003597 (2020).
118. Cao, Y. P., Bolisetty, S., Wolfisberg, G., Adamcik, J. & Mezzenga, R. Amyloid fibril-directed synthesis of silica core–shell nanofilaments, gels, and aerogels. *Proc. Natl Acad. Sci. USA* **116**, 4012–4017 (2019).
119. Mittal, N. et al. Multiscale control of nanocellulose assembly: transferring remarkable nanoscale fibril mechanics to macroscale fibers. *ACS Nano* **12**, 6378–6388 (2018).
120. Ling, S. et al. Polymorphic regenerated silk fibers assembled through bioinspired spinning. *Nat. Commun.* **8**, 1387 (2017).
121. Jolowsky, C., Sweat, R., Park, J. G., Hao, A. & Liang, R. Microstructure evolution and self-assembling of CNT networks during mechanical stretching and mechanical properties of highly aligned CNT composites. *Compos. Sci. Tech.* **166**, 125–130 (2018).
122. Huang, Y., Sasano, T., Tsujii, Y. & Ohno, K. Well-defined polymer-brush-coated rod-shaped particles: synthesis and formation of liquid crystals. *Macromolecules* **49**, 8430–8439 (2016).
123. Liu, Z., Xu, Z., Hu, X. & Gao, C. Lyotropic liquid crystal of polyacrylonitrile-grafted graphene oxide and its assembled continuous strong nacre-mimetic fibers. *Macromolecules* **46**, 6931–6941 (2013).
124. Naguib, M. Multifunctional pure MXene fiber from liquid crystals of only water and MXene. *ACS Cent. Sci.* **6**, 344–346 (2020).

125. Djumas, L., Molotnikov, A., Simon, G. P. & Estrin, Y. Enhanced mechanical performance of bio-inspired hybrid structures utilising topological interlocking geometry. *Sci. Rep.* **6**, 26706 (2016).
126. Alred, J. M., Bets, K. V., Xie, Y. & Yakobson, B. I. Machine learning electron density in sulfur crosslinked carbon nanotubes. *Compos. Sci. Technol.* **166**, 3–9 (2018).

Acknowledgements

We acknowledge support from multiple sources: D.N., the Air Force Office of Scientific Research (AFSOR), 18RXCOR060 and 22RXCOR014; K.D., ONR, N00014-18-1-2528; M.R.B., AFOSR, FA8650-19-2-5209; M.J.B., AFOSR, FATE MURI FA9550-15-1-0514; L.C.H., Office of Naval Research Global, N62909-18-1-2024; S.Keten, PECASE Award ONR, N00014-16-1-3175; G.C.S., Center for Bio-Inspired Energy Sciences (CBES), an Energy Frontiers Research Center (EFRC), under DE-SC0000989; V.V.T., Air Force Research Laboratory, FA8650-16-D-5404, AFOSR, FA9550-20-1-0305 and NSF-ECCS 2203806; L.C.B., AFOSR, FA9550-18-1-0381; J.A.E., NSF Career Award, CMMI 1454072; P.V.C., Engineering and Physical Sciences Research Council, EP/R029598/1; H.H., NSF CMMI 1940335, NSF OAC 1931587, and NASA Space Technology Research Institute, STRI-NNX17AJ32G.

Competing interests

The authors declare no competing interests.

Additional information

Correspondence should be addressed to Dhriti Nepal, Vladimir V. Tsukruk or Hendrik Heinz.

Peer review information *Nature Materials* thanks Lars Berglund, Ali Miserez, Andreas Walther and the other, anonymous, reviewer(s) for their contribution to the peer review of this work.

Reprints and permissions information is available at www.nature.com/reprints.

Publisher's note Springer Nature remains neutral with regard to jurisdictional claims in published maps and institutional affiliations.

Springer Nature or its licensor (e.g. a society or other partner) holds exclusive rights to this article under a publishing agreement with the author(s) or other rightsholder(s); author self-archiving of the accepted manuscript version of this article is solely governed by the terms of such publishing agreement and applicable law.

© Springer Nature Limited 2022

¹Materials and Manufacturing Directorate, Air Force Research Laboratory, Wright-Patterson AFB, OH, USA. ²School of Materials Science and Engineering, Georgia Institute of Technology, Atlanta, GA, USA. ³Department of Chemical and Biological Engineering, University of Colorado at Boulder, Boulder, CO, USA. ⁴Department of Materials Science and Engineering, Carnegie Mellon University, Pittsburgh, PA, USA. ⁵Department of Mechanical Engineering and Materials Science, Duke University, Durham, NC, USA. ⁶Department of Civil and Environmental Engineering, MIT, Cambridge, MA, USA. ⁷Department of Chemistry, University College London, London, UK. ⁸Department of Civil and Environmental Engineering, Carnegie Mellon University, Pittsburgh, PA, USA. ⁹Department of Mechanical Engineering, Johns Hopkins University, Baltimore, MD, USA. ¹⁰Institute for Frontier Materials, Deakin University, Waurn Ponds, Victoria, Australia. ¹¹Department of Biomedical Engineering, Tufts University, Medford, MA, USA. ¹²Department of Mechanical Engineering, Northwestern University, Evanston, IL, USA. ¹³Department of Chemical Engineering, University of Michigan, Ann Arbor, MI, USA. ¹⁴Department of Chemistry, Northwestern University, Evanston, IL, USA. ¹⁵Yusuf Hamied Department of Chemistry, University of Cambridge, Cambridge, UK. ¹⁶Department of Zoology, University of Oxford, Oxford, UK. ¹⁷Halicioğlu Data Science Institute, University of California San Diego, La Jolla, CA, USA. ¹⁸Department of Materials Science and Nanoengineering, Rice University, Houston, TX, USA. ¹⁹Department of Chemistry, Rice University, Houston, TX, USA. ✉e-mail: dhriti.nepal.1@afrl.af.mil; vladimir@mse.gatech.edu; hendrik.heinz@colorado.edu